Magnetic crust of Mars

Jafar Arkani-Hamed
Earth and Planetary Sciences, McGill University, Montreal, Quebec, Canada

Received 28 December 2004; revised 4 April 2005; accepted 15 June 2005; published 23 August 2005.

[1] The strong magnetic anomalies of Mars require highly magnetic sources in the crust. The bottom of the potentially magnetic layer is constrained by the Curie temperature of its magnetic carriers, and the top of the layer is constrained by the thickness of the uppermost crust that has been demagnetized by the impacts. This paper presents a systematic study of the thermal evolution of the Martian crust and the effects of eight major physical parameters on the thickness of the potentially magnetic layer in the crust. It is shown that the initial upper mantle temperature, the mantle viscosity, and the total radioactive content of Mars are the major parameters that have substantial effects on the thermal state of the crust in the first 1 Gyr of the planet's history. The magnetic source bodies that have been magnetized by the core field during the first 500 Myr are located in the upper about 100–90, 90–80, or 55–45 km of the crust if hematite, magnetite, or pyrrhotite is the major magnetic carrier of the source bodies, respectively. The shock pressures induced in the crust by impacts can demagnetize the uppermost part of the crust. It is demonstrated in this paper that impacts that create craters of diameters larger than ~200 km are capable of demagnetizing the entire crust, and those that create craters of diameters less than ~50 km can demagnetize the upper 10–20 km of the crust. Detailed studies of the secondary thermal remanent magnetization acquired by deeper parts of the crust, in the absence of the core field but in the presence of the magnetic field of the upper crust, suggest that the secondary magnetization has minor effects on the observed magnetic anomalies of Mars.

Citation: Arkani-Hamed, J. (2005), Magnetic crust of Mars, *J. Geophys. Res.*, *110*, E08005, doi:10.1029/2004JE002397.

1. Introduction

[2] The magnetization of the Martian crust is of remanent origin that was mainly acquired when the core dynamo was active. It is a matter of debate whether the magnetization acquired by deeper parts of the crust, in the absence of the core field but in the presence of the magnetic field of the upper parts of the crust, has appreciable contribution to the observed magnetic anomalies [*Arkani-Hamed*, 2003; *Kletetschka et al.*, 2005]. The lateral variations of magnetization in the Martian crust, which are the source of the magnetic anomalies, may arise from seafloor spreading type magnetization, from the juxtaposition of continental type blocks with different magnetization, or from intrusive bodies with magnetization different from that of the country rocks. The seafloor spreading type magnetization was suggested for somewhat elongated magnetic anomalies of Cimmeria and Sirenum Terrae [*Connerney et al.*, 1999, 2001]. Although some diagnostic tests relevant to seafloor spreading anomalies have not supported the suggestion [*Harrison*, 2000], the tests may not be conclusive for a seafloor-spreading type magnetic super chron that consists of numerous magnetic stripes with different directions of magnetization while the entire super chron has an overall dominant magnetization polarity. Intrusive bodies have been suggested for the source of some small magnetic anomalies [*Arkani-Hamed*, 2001; *Hood and Richmond*, 2002]. It remains to be verified whether large intrusive bodies are capable of producing the extensive and strong anomalies associated with Cimmeria and Sirenum Terrae, or the anomalies reflect possible juxtaposition of crustal blocks with different magnetization.

[3] It is not possible to determine detailed vertical variations of the magnetization of the Martian crust on the basis of magnetic data analysis alone. It is, however, possible to estimate the thickness of the magnetic part of the Martian crust. The main goal in this paper is to estimate the upper limit for the thickness of the potentially magnetic layer. The magnetic layer is bounded at the bottom by the depth to Curie isotherm of its major magnetic minerals, and at the top by the depth to the base of a near surface zone that has been demagnetized by impact-induced shock waves. The depth to Curie isotherm depends on the thermal state of the Martian crust. The first section presents several models for the thermal state of the Martian crust, determined through simulating the thermal evolution of Mars. The effects of different physical parameters on the depth to Curie isotherm are systematically investigated. It is demonstrated that the temperature in the region deeper than around 90 km became higher than the Curie temperature of possible magnetic minerals of the Martian crust after the cessation of the core dynamo. The thickness of the near surface zone that has been demagnetized by the impact-induced shock waves depends on the size of the projectiles that impacted Mars. The second section investigates the demagnetization of the

0148-0227/05/2004JE002397$09.00

upper parts of the crust by impact-induced shock waves. It is shown that the uppermost 10–20 km of the crust beneath major parts of Cimmeria and Sirenum Terrae is almost entirely demagnetized by the shock waves produced by impacts that have created both visible and buried craters. The third section presents a detailed study of the secondary magnetization acquired by the deeper parts of the crust in the presence of the magnetic field of the upper parts and after the core dynamo ceased to exist. Two sets of models are examined for the magnetic properties of the lower crust, a uniformly magnetic lower crust and a magnetically heterogeneous lower crust. It is concluded that the secondary magnetization has minor contributions to the observed magnetic anomalies.

2. Depth to Curie Isotherm

[4] The strong magnetic anomalies in the south hemisphere of Mars arise from the lateral variations of the bulk remanent magnetization (vertically integrated remanent magnetization). The anomalies cannot provide information about the details of the vertical variations of the magnetization, and to that matter the thickness of the layer. Other independent information is needed to constrain the potentially magnetic layer; for example, the depth to Curie isotherm defines the bottom boundary of the layer. *Nimmo and Gilmore* [2001] estimated a thickness of ~35 km for the magnetic layer of Mars on the basis of the statistical characteristics of the magnetic anomalies associated with intermediate size craters. *Voorhies et al.* [2002] suggested a source depth of ~46 km by comparing the power spectra of the magnetic fields of Earth and Mars. *Arkani-Hamed* [2002] assumed a 50 km thick nominal magnetic layer on the basis of previous thermal evolution models of Mars, and *Langlais et al.* [2004] used a 40 km thick layer.

[5] The lower boundary of the potentially magnetic layer is defined by the Curie isotherm of major magnetic minerals magnetite, hematite, and pyrrhotite which are suggested for the Martian crust on the basis of rock magnetic data [e.g., *Kletetschka et al.*, 2000, 2004; *Hargraves et al.*, 2001; *Dunlop and Kletetschka*, 2001; *Dunlop and Arkani-Hamed*, 2005]. The Curie temperature of hematite-ilmenite lamellae which is another magnetic carrier suggested for Mars [*Hargraves et al.*, 2001; *Kletetschka et al.*, 2002] is similar to that of magnetite [*Robinson et al.*, 2002]. Curie temperatures of 853K, 943K and 593K are used for magnetite, hematite and pyrrhotite in the present paper. Time evolution of depth to Curie temperature of these minerals must be estimated not only during the active period of the core dynamo, but also after the cessation of the dynamo.

[6] In this study, an upper limit is estimated for the depth to the bottom of the potentially magnetic layer on the basis of the thermal evolution models of Mars. The thermal evolution of Mars is poorly understood, and remains speculative. Whether appreciable plate tectonics were active during the early history of Mars or the planet essentially started as a one-plate planet is still debated [*Sleep*, 1994; *Spohn et al.*, 2001; *Breuer and Spohn*, 2003]. If plate tectonics were significant, for example, as active as that examined by *Breuer and Spohn* [2003], then the crust was being formed at the ridge axes and being consumed at the trenches in a short time without appreciable cooling of its deeper part. The residing time of a plate at the surface was short, and the magnetic layer was thin. The plate tectonics cooled the interior of the planet efficiently, but retained a thin magnetic layer at the surface. If, on the other hand, no plate tectonics occurred, a growing stagnant lid at the surface hampered heat loss from the mantle while its outer parts cooled significantly, resulting in a thick magnetic layer when the core dynamo was active. In accordance with the premise of determining an upper limit for the thickness of the potentially magnetic layer, a buoyant crust is assumed in the thermal evolution models to represent an initial crust. The effect of mantle solidification on the thermal evolution is ignored. The solidification releases the latent heat and reduces the cooling rate of the planet, hampering the thickening of the magnetic layer.

[7] Thermal evolution of Mars has been investigated in the last three decades using parameterized convection simulations. The emphasis has been on the history of the core dynamo [*Stevenson et al.*, 1983], the effects of possible early plate tectonics on the thermal state of the interior [*Nimmo and Stevenson*, 2000], the effects of temperature on the internal structure [e.g., *Spohn et al.*, 2001; *Breuer and Spohn*, 2003], and the creation and growth of the crust [*Hauck and Phillips*, 2002]. Except for a limited study [*Arkani-Hamed*, 2003], the effect of the thermal evolution on constraining the bottom of the potentially magnetic layer of Mars has not been investigated.

[8] The thermal evolution models of Mars presented in this paper are calculated using parameterized convection calculations in a stagnant lid regime with a growing stagnant lid on the surface. Briefly, the Martian interior is divided into five regions: a vigorously convecting core of radius R_c with adiabatic temperature distribution, a conducting lower thermal boundary layer of outer radius R_m, the convecting part of the mantle of outer radius R_u where adiabatic temperature prevails, the conducting upper thermal boundary layer of outer radius R_l, and the overlying conducting stagnant lid of outer radius R, the Martian radius. Except for R_c and R the locations of the other boundaries are time dependent. In the convecting regions the adiabatic temperature prevails. In the conducting regions the spherically symmetric conduction equation with temperature dependent thermal conduction and time dependent heat generation is solved. The energy balance in the core is

$$4\pi R_c^2 F_c = -4\pi \int_o^{Rc} \rho_c C_c (\Delta T_c/\Delta t) r^2 \, dr + Q_c, \qquad (1)$$

where F_c is the heat flux out of the core, ρ_c is the core density, C_c (800 J/kg/K) is the specific heat of the core, ΔT_c is the increase in the adiabatic temperature T_c within a time interval of Δt, r is the radial distance form the center, and Q_c is the rate of heat generation in the core. The time variations of the adiabatic temperature in the core is related to the time variations of temperature at the core mantle boundary T_{cm},

$$\Delta T_c/\Delta t = \mathrm{Exp}\left(\int_r^{Rc} \alpha_c g_c/C_c dr\right) \Delta T_{cm}/\Delta t, \qquad (2)$$

where α_c (7×10^{-5}) and g_c are the thermal expansion coefficient and the gravitational acceleration in the core.

The energy balance in the convecting part of the mantle is

$$4\pi R_u^2 F_u = 4\pi R_m^2 F_m + 4\pi/3\left(R_u^3 - R_m^3\right)q_m - 4\pi \int_{Rm}^{Ru} \rho_m C_m(\Delta T_m/\Delta t) r^2 \, dr, \quad (3)$$

where F_m and F_u are heat flux at the top of the bottom boundary layer and at the bottom of the top boundary layer, respectively, q_m is the rate of heat generation per unit volume in the mantle, ρ_m is the mantle density, C_m (1200 J/kg/K) is the specific heat of the mantle, ΔT_m is the increase in the adiabatic temperature T_m of the mantle within a time interval of Δt, and r is the radial distance from the center. The time variations of the adiabatic temperature in the mantle is related to the time variations of the temperature at the bottom of the upper thermal boundary layer T_u, by

$$\Delta T_m/\Delta t = \mathrm{Exp}\left(\int_r^{Ru} \alpha_m g_m/C_m dr\right)\Delta T_u/\Delta t, \quad (4)$$

where α_m and g_m are the thermal expansion coefficient and gravitational acceleration in the mantle. Note that among the physical parameters entering these equations only the specific heat is constant. The radioactive heat sources are time dependent but uniformly distributed in the mantle, as well as in the crust but with different concentrations. Each of the radioactive elements, ^{235}U, ^{238}U, ^{232}Th, and ^{40}K decay according to their half-lives. In both thermal boundary layers as well as in the stagnant lid the spherically symmetric heat conduction equation is solved by

$$\rho C(\Delta T/\Delta t) = 1/r^2 \, d/dr\left(r^2 K \, d/dr \, T\right) + q, \quad (5)$$

where ρ, C (1200 J/kg/K), T, K, and q stand for density, specific heat, temperature, thermal conductivity and rate of heat generation per unit volume in those regions. Continuous temperature and heat flux conditions are imposed at the boundaries, except for the stagnant lid where the upper surface of the lid is put to a fixed temperature of the Martian surface. The convection simulation is made only in the convecting part of the Mantle located between the upper and lower boundary layers. *Breuer and Spohn* [2003] compared plate-tectonic and stagnant lid thermal evolution models of Mars and concluded that early plate tectonics cool the interior efficiently and do not allow sufficient production of the crust. They favored stagnant lid thermal evolution scenario. *Solomatov* [1995] studied the convective regime in planetary interior where viscosity varies several orders of magnitude. He concluded that as the viscosity contrast in the mantle increases the convective region passes from small viscosity contrast regime to transition regime and finally to stagnant lid regime. *Moresi and Solomatov* [1995] showed that the stagnant lid regime starts when the viscosity contrast becomes larger than 10^4–10^5. An interesting conclusion of the stagnant convection models is the fact that the stagnant lid thickness is laterally variable, thinner over the upwelling and thicker over the down going mantle. However, such variations cannot be incorporated in the spherically symmetric parameterized convection models. Moreover, there is no information about the actual locations of the upwelling and down going mantle of Mars, which is especially the case during the first about 500 Myr of the planet's history, the main concern in this paper. For numerical accuracy the crust and mantle are divided into layers of 1 km thickness, and the core into layers of 10 km thickness.

[9] The Mars models are differentiated during or shortly after accretion and produced a buoyant initial crust overlying a mantle that in turn overlies an iron-rich core. Whether the major part of the Martian crust (20–30 km) was formed during the early chemical differentiation and the remaining part was subsequently formed gradually [*Norman*, 1999, 2002], or the entire crust was formed gradually in the first ~1 Gyr [*Hauck and Phillips*, 2002] is not yet clear. The Hf and W isotope analyses of the Martian meteorites suggest that the chemical differentiation and the core formation in Mars probably occurred within 20–30 Myr of the planet's history [*Halliday et al.*, 2001]. The observed W isotope anomaly of Mars suggests that a significant amount of crust was formed during an early chemical differentiation [e.g., *Jagoutz*, 1991; *Harper et al.*, 1995; *Borg et al.*, 1997; *Blichert-Toft et al.*, 1999], and major part of the crust has not been incorporated in the mantle recycling processes [*Halliday et al.*, 2001]. The initial chemical differentiation has likely partitioned an appreciable amount of radioactive elements in the initial crust. *McLennan* [2001] suggested that ~75% of the radiogenic elements are initially concentrated in a crust of ~50 km thickness. I examine different partitioning coefficients to illustrate the effect of radioactive concentration in the crust on the potentially magnetic layer. The remaining radioactive elements are uniformly distributed in the mantle. No subsequent gradual addition of crustal material is taken into account. The underlying lithosphere that is added to the stagnant lid has the same concentration of radioactive elements as the entire mantle. Adding newly formed crustal material with high concentration of radioactive elements to the crust enhances the radioactive elements directly beneath the initial crust and hampers cooling of the crust in the early stages when the core dynamo existed. No core solidification is considered because the core most likely did not initiate solidification in the first ~500 Myr, the period we are most concerned with.

[10] The initial temperature linearly increases in the upper parts of Mars, starting with a surface temperature of 230K and a given temperature at the base of the upper thermal boundary layer. If water existed on the surface in the early history of the planet, the surface temperature must have been ~ 280K. The lower surface temperature adopted here cools the crust efficiently, which is in accordance with our goal of estimating the upper limit for the potentially magnetic layer. The initial temperatures in the mantle and core adiabatically increase with depth.

[11] Different values are used for the major physical parameters in order to investigate their effects on the thickness of the potentially magnetic layer. The initial crustal thickness of 10 to 50 km are considered to span the thickness range estimated from chemical differentiation [*Norman*, 2002], gravity and topography data [*Zuber et al.*, 2000], and theoretical modeling [*Hauck and Phillips*, 2002].

Table 1. Radioactive Models[a]

Model	U	Th/U	K/U
Wänke and Dreibus [1994]	16	3.5	19,062
Lodders and Fegley [1997]	16	3.4	57,500
Terrestrial	30	4.0	10,000

[a]The U values are the present mean concentration in ppb.

The initial upper mantle temperatures used, 1600–1800 K, include the solidus temperature of mantle material [e.g., *Lesher et al.*, 2003; *Matsukage and Kubo*, 2003] and are comparable with the values used by *Hauck and Phillips* [2002]. Much higher temperatures, 2000–2100 K, have also been used by other investigators [e.g., *Schubert and Spohn*, 1990; *Spohn et al.*, 2001; *Breuer and Spohn*, 2003]. The initial temperature at the core-mantle boundary is based on the continuity of the mantle and core temperature at that boundary. A superheated core model is also examined where the initial temperature of the core is increased by 300K, as adopted by *Spohn et al.* [2001]. Different values have been estimated for the total content of the radioactive elements [*McDonough and Sun*, 1995; *Schubert and Spohn*, 1990; *Wänke and Dreibus*, 1994; *Lodders and Fegley*, 1997]. The models of *Wänke and Dreibus* [1994] and *Lodders and Fegley* [1997] and a terrestrial model [*Turcotte and Schubert*, 1982] are examined. Table 1 lists the radioactive elements in the models. No radioactive elements except for potassium are allowed in the core. The core radius is taken to be 1500 km. Three different models of the thermal expansion coefficient α are examined for the mantle: constant, ($\alpha = \alpha_o = 3 \times 10^{-5}$), linearly decreasing with depth ($\alpha = \alpha_o r/R$), and decreasing with depth as a square of radial distance ($\alpha = \alpha_o r^2/R^2$), where R is the radius of Mars and r is the distance from the center of Mars. Also the experimentally measured temperature-dependent thermal conductivity model of olivine [*Schatz and Simmons*, 1972] is used for the thermal conductivity of the stagnant lid and the thermal boundary layers in the mantle.

[12] The dynamic viscosity, η, is assumed temperature and pressure dependent,

$$\eta = \eta_o \exp[(E + VP)/RT], \tag{6}$$

where E (=300 KJ/mole) is the activation energy, V ($=2.5 \times 10^{-6}$ m^3/mol) is the activation volume, P is the pressure, R (=8.3144) is the gas constant, T is the temperature, and η_o ($= 6.05 \times 10^{10}$ Pa s) is a constant. These parameter values result in a dynamic viscosity of 10^{20} Pa s at 1700 K temperature in the upper mantle of Mars. The viscosity increases with depth because of its pressure dependence. The pressure is determined using an internal density model similar to those of *Van Hoolst et al.* [2000] that satisfies the total mass and the moment of inertia factor, 0.365, of Mars, and has phase transitions from olivine to spinel in the mid-mantle and spinel to prevoskite in the deeper part of the mantle near the core mantle boundary. Figure 1 shows the density model used and the resulting pressure and gravitational acceleration inside the spherically symmetric Mars model. The pressure is calculated assuming hydrostatic equilibrium.

[13] The strong increase of viscosity in the cold regions near the surface results in a stagnant lid on top of the convecting interior. The stagnant lid convection regime of an incompressible fluid with temperature-dependent viscosity, where viscosity changes by many orders of magnitude, shows that the dynamics of the convecting layer underlying the stagnant lid can be approximated by constant viscosity convection regime [*Moresi and Solomatov*, 1995]. The temperature at the base of the stagnant lid, T_l, is related to the internal temperature, T_m, through

$$T_l = T_m(1 - \beta R T_m/E), \tag{7}$$

where β ($\sim$2.23) is a constant [*Grasset and Parmentier*, 1998]. In the parameterized convection models considered in this paper, the Martian mantle is compressible and temperature in the interior is no longer constant. It increases by about 250–300 K across the adiabatic convecting region. In adopting this equation to the parameterized convection models, T_m is taken to be the temperature at the uppermost part of the adiabatic region, T_u. The temperature at the base of the stagnant lid is determined at each time step using equation (7). Equal time steps of 50,000 years are adopted in the calculations. In the models presented here, the initial stagnant lid consists of an initially buoyant crust and the uppermost part of the mantle. The stagnant lid grows in time and includes deeper parts of the uppermost mantle at later stages as the upper mantle cools and becomes rigid.

[14] The thickness of the upper thermal boundary layers is determined on the basis of the convection instability in the layer

$$\delta = [\eta \kappa R_{cr}/\alpha \rho g \Delta T]^{1/3}, \tag{8}$$

where η is calculated at Tu, κ is the mean thermal diffusivity of the layer, and ΔT is the temperature difference across the layer ($T_u - T_l$). R_{cr} is the critical Rayleigh number of the layer. The upper thermal boundary layer has a rigid upper boundary and a free lower boundary. A critical Rayleigh number of 1300 is adopted on the basis of the theoretical

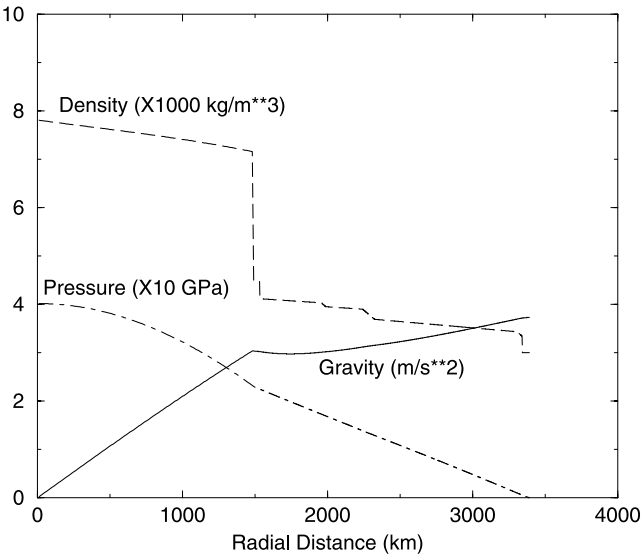

Figure 1. The density model of Mars adopted in this study. The gravity and pressure are calculated on the basis of the density model, assuming hydrostatic equilibrium.

Table 2. Physical Parameters of the Nominal Model

Parameter	Value/Source
Radius	3390 km
Core radius	1500 km
Initial thickness of the crust	30 km
Specific heat of the mantle	1200 J/kg/K
Specific heat of the core	800 J/kg/K
Thermal expansion coefficient, mantle	3×10^{-5}
Thermal expansion coefficient, core	7×10^{-5}
Surface temperature	230 K
Elastic-ductile transition temperature	1073 K
Radioactive element content	*Wänke and Dreibus* [1994]
Radioactive content of the crust	30%
Potassium content of the core	0

calculations by *Stengel et al.* [1982] for fluids with viscosity that depends on temperature exponentially. The lower thermal boundary has a free lower and a free upper boundaries and a critical Rayleigh number of 500 is used (see Figure 2 of Stengel et al. for both of these values).

[15] A total of 23 models are calculated in order to examine the effects of different physical parameters on the thickness of the potentially magnetic layer. The nominal model will be described in some detail. Table 2 lists the physical parameters of this model. The differences between the nominal model and the others will be discussed in the context of the effects of different physical parameters on the thickness of the potentially magnetic layer. The nominal model has an initial crust of 30 km thickness that contains 30% of the radioactive elements of the entire planet. *Wänke and Dreibus* [1994] model is used for the concentration of radioactive elements. The initial temperature increases linearly from the surface temperature of 230 K to 1700 K at the base of the upper thermal boundary layer of the mantle, below which temperature increases adiabatically with depth in the lower parts of the mantle, by about 300 K. The initial temperature is continuous at the core mantle boundary and adiabatically increases with depth in the core. The crust and mantle have equal and constant thermal expansion coefficient, α_o. Figure 2 shows the upper mantle temperature at 400 km depth and the temperature at the core mantle boundary throughout the thermal evolution of the nominal model. The upper mantle temperature increased within the first about 1 Gyr because of radioactive internal heating and thermal blanketing effect of the stagnant lid, but then decreases monotonically with time, similar to the mantle temperature of stagnant lid model by *Spohn et al.* [2001]. The core temperature increases in the first about 2.5 Gyr, because mantle is heating the core, as reflected in the negative heat flux out of the core (Figure 3). Heat flux at the surface shows a sharp rise in the very early times because of huge amount of heat produced by the radioactive elements in the crust. The heat flux resumes a steady decay with time after about 200 Myr. Figure 4 shows the temperature profiles in the stagnant lid within the first 500 Myr. We note that while the stagnant lid is heated up it also thickens within this period, which is the natural consequence of the inefficient heat loss from the mantle in the stagnant lid convection regime. The stagnant lid of the nominal model thickens monotonically within the first about 500 Myr, and then thins until about 2 Gyr before resuming its final monotonic thickening in later times (Figure 5), which is similar to the stagnant lid STL21 model of *Breuer and Spohn* [2003, Figure 3]. The stagnant lid consists of an upper elastic part and a lower ductile part. For an elastic-ductile transition temperature of 1050 K, the elastic layer of the nominal model at present is about 146 km, which is comparable to the elastic layer deduced from gravity and topography data [e.g., *Solomon and Head*, 1990; *Arkani-Hamed*, 2000; *McGovern et al.*, 2002].

[16] Included in Figure 5 are the depths to Curie isotherms of hematite, magnetite and pyrrhotite, delineating the bottom of the potentially magnetic layer. Depth to the Curie temperature of pyrrhotite is about 1/2 that of magnetite, and depth to hematite's Curie isotherm is about 20 percent more than that of magnetite. These relative depth values are expected because of the almost linear temperature profiles

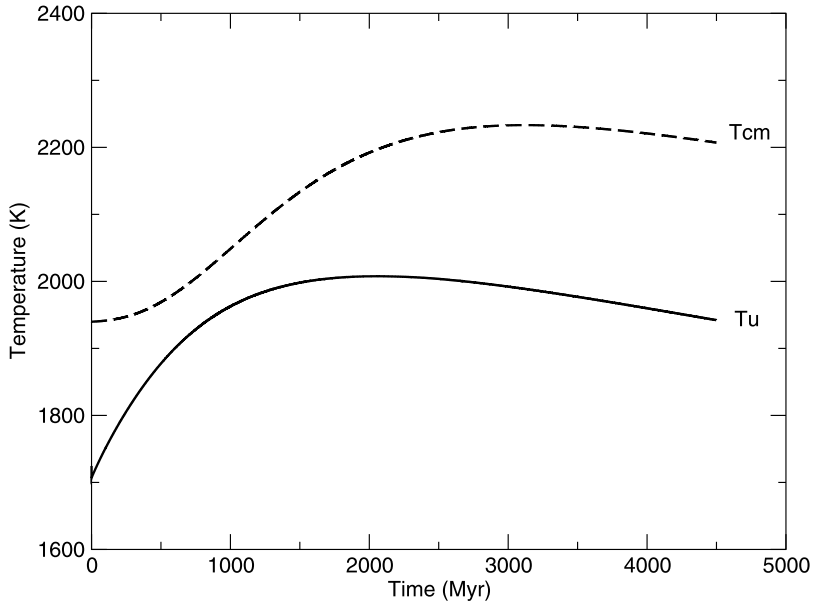

Figure 2. The upper mantle temperature, Tu, and the temperature at the core-mantle boundary, Tcm.

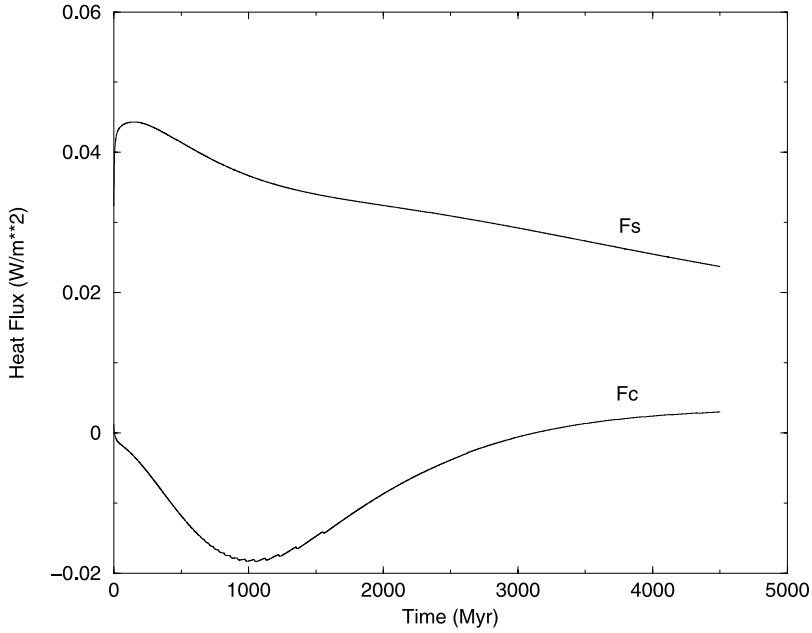

Figure 3. The heat flux at the surface, Fs, and at the core mantle boundary, Fc, for the nominal model.

in the stagnant lid. Hereafter the magnetite isotherm will be used for illustration purposes. The potentially magnetic layer of the nominal model is about 100 km in the early stages of the evolution of the planet, but it thins, reaching a minimum value at ∼200 Myr. There is minor changes in the thickness of the potentially magnetic layer after this period until about 2 Gyr, but monotonically thickens then after.

[17] The effects of eight physical parameters on the thermal evolution of Mars, and thus on the thickness of the potentially magnetic layer, are estimated. Table 3 lists the values of the major physical parameters used in the models. The models are identical to the nominal model except for these parameter values. Here I discuss the parameters that have major effects on the thickness of the potentially magnetic layer. Figure 6 shows the depth to Curie isotherm of magnetite for several sets of models. Models 2, 4, 18, and 20 are identical to the nominal model, Model 9, except for the thickness of their initial curst. We note that the crust in all these models contain 30% of the entire radioactive elements of the planet. The heat genera-

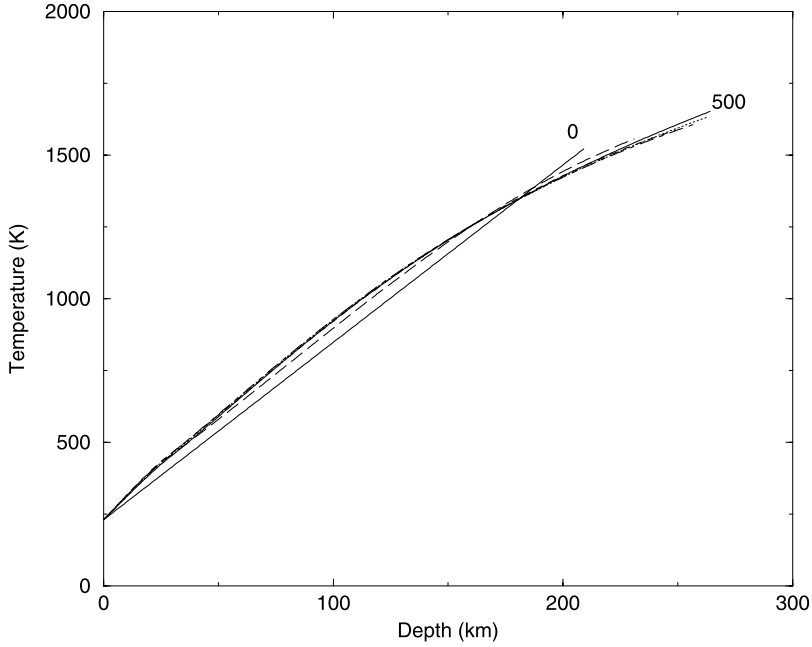

Figure 4. Snapshots of the temperature profiles in the stagnant lid of the nominal model during the first 500 Myr of the planet's history. The numbers on the curves show the time in Myr; only 0 and 500 are shown.

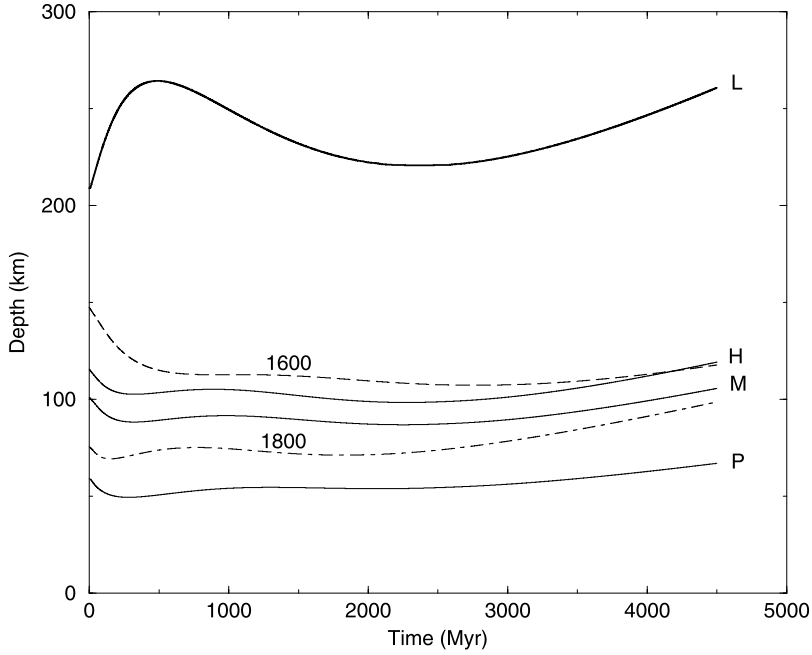

Figure 5. The Curie isotherms of hematite, H, magnetite, M, and pyrrhotite, P, in the crust of the nominal model. The dashed curves are the Curie isotherm of magnetite for models 5 and 17. The thick solid curve denoted by L is the thickness of the stagnant lid of the nominal model.

tion per unit volume of Model 2 with a 10 km thick initial crust is 5 times greater than that of Model 20 with 50 km thick initial crust. Despite strong enhancement of the heat generation per unit volume, the models with thinner crust have thicker magnetic layers (Figure 6a) because the heat produced in the crust readily escapes the planet. Models 7, 8, and 13 are identical to the nominal model except for the concentration of radioactive elements in their initial crust, which varies from 10% to 40% of the entire planet. The heat generation per unit volume in the crust of Model 7 is 4 times less than that of Model 13. The high rate of heat generation in the mantle of Model 7 enhances the mantle temperature and decreases the thickness of the potentially magnetic layer (Figure 6b). The excess heat produced in the highly radioactive crust of Model 13 readily escapes the planet without having appreciable effects on the thermal state of the crust. The thermal expansion coefficient models have substantial effects on the thermal gradient in the mantle. The highest gradient is produced by the nominal model, which has a constant thermal expansion coefficient, compared to that produced by Model 10 with linearly decreasing coefficient with depth, and more so that produced by Model 11 with power 2 decrease of the coefficient with depth. However, the effects of the depth dependent thermal expansion coefficient on the potentially magnetic layer are less than those of the other parameters discussed above (Figure 6c).

[18] The most effective parameters are the initial temperature of the upper mantle, the total radioactive content of the planet, and the viscosity of the mantle. Models 5 and 17 are identical to the nominal model except for their initial upper mantle temperature. The lower is the upper mantle temperature of a model the deeper is its Curie isotherm (Figure 6d). The differences in the thickness of the potentially magnetic layers are reduced at later times. Models 14 and 15 are

Table 3. Physical Parameters of the Thermal Evolution Models[a]

Model	1	2	3	4	5	6	7	8	9
1	10	E300	1700	0	16	1	10	0	0
2	10	E300	1700	0	16	1	30	0	0
3	20	E300	1700	0	16	1	20	0	0
4	20	E300	1700	0	16	1	30	0	0
5	30	E300	1600	0	16	1	30	0	0
6	30	E300	1700	0	16	0	30	0	0
7	30	E300	1700	0	16	1	10	0	0
8	30	E300	1700	0	16	1	20	0	0
9 Nominal	30	E300	1700	0	16	1	30	0	0
10	30	E300	1700	0	16	1	30	0	1
11	30	E300	1700	0	16	1	30	0	2
12	30	E300	1700	0	16	1	30	15	0
13	30	E300	1700	0	16	1	40	0	0
14	30	E300	1700	0	16	2	30	0	0
15	30	E300	1700	0	30	0	30	0	0
16	30	E300	1700	300	16	1	30	0	0
17	30	E300	1800	0	16	1	30	0	0
18	40	E300	1700	0	16	1	30	0	0
19	40	E300	1700	0	16	1	40	0	0
20	50	E300	1700	0	16	1	30	0	0
21	50	E300	1700	0	16	1	50	0	0
22	30	E540	1700	0	16	1	30	0	0
23	30	$\eta/5$	1700	0	16	1	30	0	0

[a]The columns are as follows: 1, initial crustal thickness in km; 2, E300 denotes the activation energy of 300 KJ, E540 denotes that of 540 KJ, and $\eta/5$ means that the dynamic viscosity is 1/5 of that of the nominal model; 3, initial temperature at the bottom of the upper thermal boundary layer in K; 4, the super heated core of 300 K extra; 5, the average uranium content at present in ppb; 6, the radioactive model (1, *Wänke and Dreibus* [1994]; 2, *Lodders and Fegley* [1997], and 0, *Turcotte and Schubert* [1982]); 7, the percentage of the total radioactive elements of the planet concentrated in the crust; 8, the percentage of potassium of the total planet concentrated in the core; and 9, thermal expansion coefficient (0, constant (3×10^{-5})); 1, linearly increasing with radial distance; and 2, quadratically increasing with the radial distance.

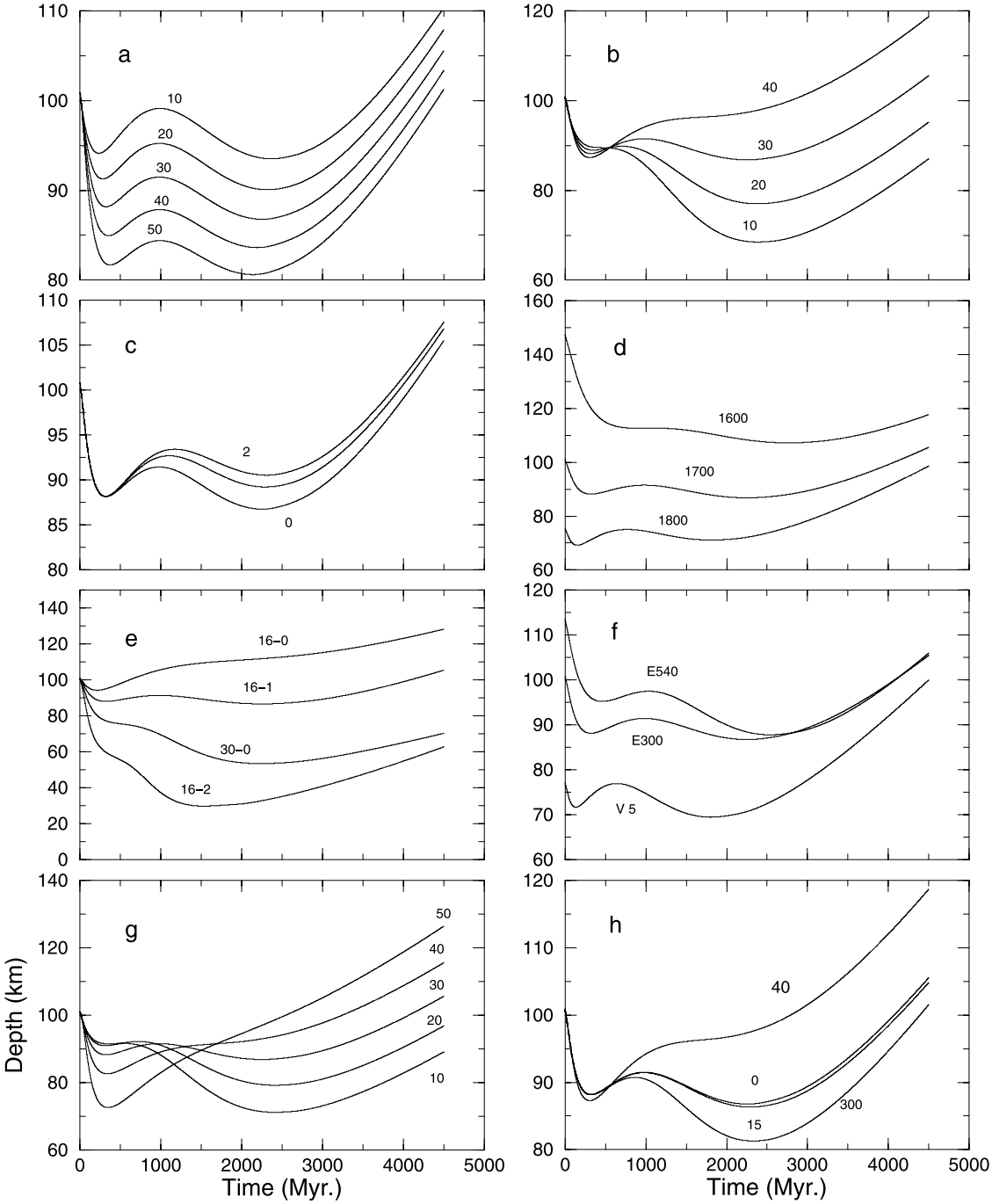

Figure 6. The depth to the Curie isotherm of magnetite. The numbers on the curves are as follows: (a) the thickness of the initial crust (km), (b) the radioactive elements concentrated in the crust (%), (c) the depth dependence of the thermal expansion coefficient, the curves 1 and 2 denoting the linear and quadratic decrease with depth, (d) the initial temperature in the upper mantle at the bottom of the upper thermal boundary layer, (e) the first number is the ppb average uranium content of the planet at present, and the second number is 0 for terrestrial ratios of Th/U and K/U, 1 for the *Wänke and Dreibus* [1994] model, and 2 for the *Lodders and Fegley* [1997] model, (f) the activation energy of the nominal model, and Model 22, V5 denoting Model 23, (g) models with identical rate of heat generation per unit volume in the crust, and (h) the number 15 is the percentage of the total potassium in the core, 300 is the excess degree of the superheated core, and 40 is the percentage of the total radioactive elements partitioned to the crust.

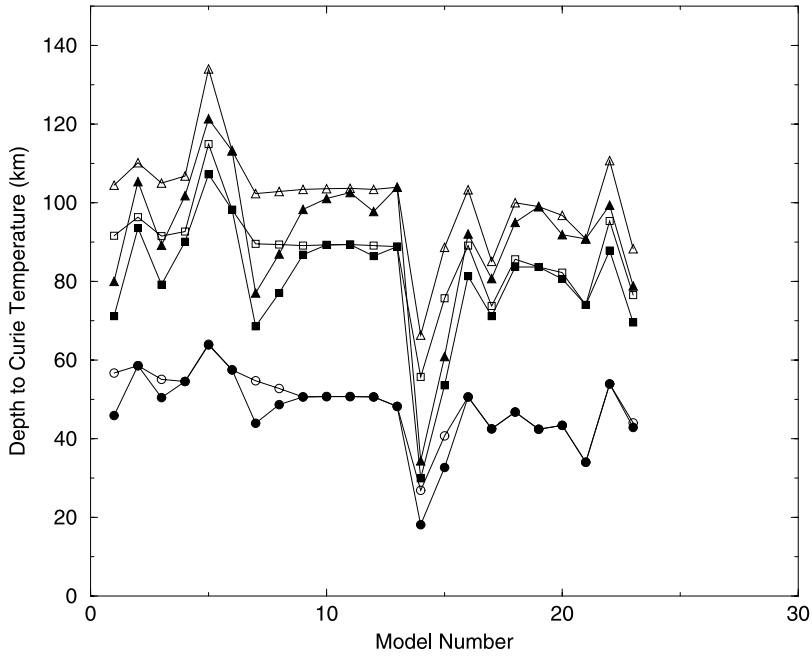

Figure 7. The depth to the Curie isotherms of hematite (triangle) magnetite (square) and pyrrhotite (circle). The open symbols are at 500 Myr, and the solid ones are the minimum values attained during the entire thermal evolution of the models.

identical to the nominal model except for their total radioactive contents. The higher the radioactive content the shallower is the Curie isotherm (Figure 6e). Model 6 is identical to the nominal model except for its Th/U and K/U ratios which are assumed terrestrial like. This model has the thickest potentially magnetic layer, whereas Model 14 with enhanced radioactive content has the thinnest layer. To investigate the effects of mantle viscosity the activation energy, E, and the constant factor of viscosity, η_o, are changed. Adopting higher activation energy of 540 KJ/mol [*Grasset and Parmentier*, 1998] without changing η_o increases the upper mantle viscosity by $\sim$7 orders of magnitude. To obtain an upper mantle viscosity similar to that of the nominal model η_o is reduced to 2.56×10^3 Pa s. The potentially magnetic layer of the resulting Model 22 is slightly thicker than that of the nominal model in the first about 1.5 Gyr, but the differences diminish at later times (Figure 6f). Also shown in Figure 6f is the thickness of the potentially magnetic layer of Model 23, which is identical to the nominal model except for the constant factor of its viscosity, η_o, which is reduced by a factor of 5. The low viscosity of its upper mantle enhances the heat flux to the stagnant lid, and thus results in a thinner stagnant lid as well as the potentially magnetic layer compared to those of the nominal model.

[19] Other parameters such as the heat sources in the core or super heated initial core have minor effects on the thickness of the potentially magnetic layer. Figure 6h shows the depth to Curie temperature of models 12, and 16 that are identical to the nominal model except for their core, which either has internal heat sources due to potassium content (15% of the total potassium of the planet) or an initially higher temperature, by 300 K, than that of the nominal model. Included in the figure is the Curie isotherm of Model 13 that is identical to the nominal model except that 40%, instead of 30%, of the radioactive materials is concentrated in the crust. The model has thicker magnetic layer. Figure 6h emphasizes that removing only 10% extra radioactive elements from the mantle and putting it in the crust has by far more effects on the potentially magnetic layer than putting as much as 15% potassium in the core or having a hotter initial core by 300 K.

[20] The potentially magnetic layers of all of the models are presented in a single figure (Figure 7) that allows better comparison of the models and assessing the effects of the parameters on the thickness of the potentially magnetic layer. Included in Figure 7 are the depths to the bottom of the potentially magnetic layers for the three major magnetic carriers. The open symbols are the depths at 4 Gyr ago. The solid symbols denote the potentially magnetic layers when the layers attained their minimum thickness. Except for Model 5 and Model 14, the potentially magnetic layers of the models are comparable, suggesting a magnetic layer of around 80–90 km if magnetite is the major magnetic carrier. Model 5 is identical to the nominal model except for an initially cold upper mantle of 1600 K. The colder upper mantle reduces the temperature of the stagnant lid to lower than that of the nominal model in the early stages of evolution, and results in a thicker potentially magnetic layer. Model 14 is identical to the nominal model except for its higher concentration of radioactive elements where *Lodders and Fegley*'s [1997] radioactive concentration model is adopted. The high heat production enhances the mantle temperature, resulting in a thinner potentially magnetic layer. Figure 7 shows that for majority of the models the bottom of the potentially magnetic layer is at around 100, 85 or 50 km if hematite, magnetite or pyrrhotite is the major magnetic carriers, respectively.

[21] As mentioned earlier, the thickness of the crust in a given model remained unchanged throughout the evolution of the model. The stagnant lid initially consisted of the initial crust and part of the uppermost mantle. As time passed, and the upper part of the mantle cooled, the stagnant lid thickened by incorporating the colder part. However, the mantle part of the stagnant lid had relatively lower radioactive concentration than the crust. It is likely that the Martian crust with a high concentration of radioactive elements grew gradually in time [*Hauck and Phillips*, 2002]. Figure 6g provides an estimate of the effect of a gradually thickening crust on the thickness of the potentially magnetic layer. The figure shows the depth to Curie isotherm of magnetite for five different models, 1, 3, 9, 19, and 21, with identical heat generation per unit volume in the crust. For example, the crust of Model 1 is 10 km thick and contains only 10% of the total radioactive elements of the planet, and the crust of Model 21 is 50 km thick and contains 50% of the total radioactive elements. The radioactive heat generated in the deeper parts of the thicker curst, Model 21 and Model 19, does not readily escape and thus heats up the lower parts of the crust in the early history. But as time passes and the planet cools the mantle of the models with thicker crust gets colder because appreciable amounts of heat sources are concentrated in their crust. Except for Model 21 and to lesser extent for Model 19, the depth to the Curie isotherm of magnetite is essentially the same for the models during the active period of the core dynamo. If the crust has gradually grown from say 10 km to 50 km during the active period of the core dynamo, the depth to the Curie isotherm may have decreased by about 10 km.

[22] The crust has likely kept accreting and increasing in thickness after the core dynamo ceased to exist [*Hauck and Phillips*, 2002]. *Sohl and Spohn* [1997] presented two end-member models of Mars' internal structure, one satisfied the geochemical data derived from the SNC meteorites in terms of the bulk chondritic ratio Fe/Si = 1.71, while the other satisfied the moment of inertia factor of Mars, 0.366. The models required basaltic crustal thicknesses of 250 and 100 km. Analysis of the gravity and topography data of Mars suggest a mean crustal thickness of about 50 km, but considerably thicker crust beneath Cimmeria and Sirenum Terrae and much thinner crust beneath the northern lowlands [*Zuber et al.*, 2000]. A 90 km thick crust is proposed by *Turcotte et al.* [2002], and an upper bound of 100 km by *Nimmo and Stevenson* [2000].

3. Impact Demagnetization of the Uppermost Crust

[23] The absence of the magnetic anomalies over the giant basins of Mars led *Acuna et al.* [1999] to suggest that the crust beneath the basins is demagnetized by the impact events. Subsequent quantitative investigation of the impact-induced shock wave demagnetization showed that the giant impacts are indeed capable of demagnetizing the entire crust within ~0.8 radius of the basins and partially demagnetizing the crust to distances of about 1.4 radius [*Mohit and Arkani-Hamed*, 2004], and possibly farther out [*Hood et al.*, 2003; *Kletetschka et al.*, 2004]. However, no systematic investigation has been carried out on the impact-induced demagnetization of the uppermost crust of Mars on a global basis. In this section the shock pressure distribution in the lithosphere produced by small and intermediate size impacts is calculated to estimate the average depth of the demagnetized zone beneath Cimmeria and Sirenum Terrae. I adopted the method used by *Mohit and Arkani-Hamed* [2004] for intermediate size craters. Briefly, an observed crater diameter, D_o, is related to the transient diameter of the crater, D_{tr}, using the *Holsapple* [1993] scaling relationship

$$D_{tr} = 0.7576\, D_o^{0.921} D_*^{0.072}, \tag{9}$$

where D_* is the transition diameter from simple to complex crater, assumed 7 km for Mars [*Melosh*, 1989]. The transient crater diameter is then related to the kinetic energy of the projectile, E, through the *Schmidt and Housen* [1987] relationship

$$E = \left\{ \left(D_{tr}\, U^{0.09}\, g^{0.22} \right) / 0.2212 \right\}^{(1/0.26)}, \tag{10}$$

where U is the impact velocity, and g is the gravitational acceleration at the surface of Mars. Majority of craters on Mars are circular, they have been produced by heliocentric projectiles. Here projectile velocities of 8–12 km/s are used, which have been proposed for the heliocentric Martian impacts [*Neukum and Wise*, 1976]. Assuming a spherical projectile of basaltic composition, with density 2900 kg/m^3, the projectile kinetic energy is related to its radius, R_{pr}, which in turn is related to the radius of the isobaric core, R_o = 0.75 R_{pr}, and penetration depth of the projectile, assumed equal to R_{pr}. The Hugoniot equation [*Melosh*, 1989],

$$P_o - P'_o = \rho\, u_s\, u_p, \tag{11}$$

together with a power law distribution of shock pressure outside the isobaric core,

$$P(r) = P_o (r/R_o)^{-n}, \quad r > R_o, \tag{12}$$

and the empirical relationship between the particle velocity, u_p, and shock wave velocity, u_s,

$$u_s = C + s\, u_p, \tag{13}$$

yield the shock pressure, P(r), as a function of distance r from the center of the crater, the impact site, and the pressure in the isobaric core, P_o. The unshocked pressure P'_o is assumed to be negligible compared to the isobaric core pressure. C is the bulk sound speed (=3.5 km/s) and s (=1.5) is the shock parameter of the material [*Melosh*, 1989]. Two different exponential decay models are adopted. A constant n value of 1.87 [*Melosh*, 1989], and different n values for different pressure ranges; n = 1.2 for $P < P_H$, and for $P > 10\ P_H$, and n = 2.5 for other pressures [*Mitani*, 2003]. P_H denotes the pressure at the Hugoniot elastic limit. Also the pressure reduction near the surface due to interference of the direct and reflected waves [*Melosh*, 1989] is taken into consideration. The effective pressure at a given point in the target is calculated by

$$P_{eff} = P - P_{ref}(1 - t/t_{rise}) \quad \text{for } t < t_{rise} \tag{14a}$$

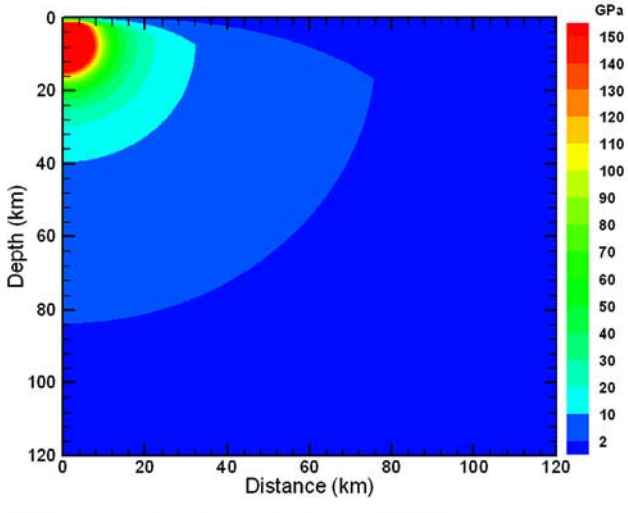

Figure 8. The shock pressure (GPa) distribution in the lithosphere produced by an impact that creates a 200 km diameter crater.

and

$$P_{eff} = P \quad \text{for } t \geq t_{rise}, \tag{14b}$$

where P is the pressure of the direct shock wave, P_{ref} is the pressure of the shock wave that is reflects at the surface, t is the difference in the arrival times of the direct and reflected waves (reflected minus direct), and t_{rise} is the risetime of the shock pressure, which is approximated by the time required for the projectile to penetrate to its final depth that is equal to the radius of the projectile [*Melosh*, 1989]. Comparison of magnetic anomalies over areas surrounding the giant impacts Hellas, Isidis, and Argyre and the calculated distribution of shock pressures showed that the crust is almost completely demagnetized at pressures higher than ~3 GPa [*Mohit and Arkani-Hamed*, 2004]. This is probably more conservative, demagnetizing pressures as low as ~1 GPa have been proposed by other investigators [e.g., *Hood et al.*, 2003].

[24] Figure 8 shows the shock pressure distribution induced by a projectile that creates a crater of 200 km diameter. The parameter n value of 1.87 is adopted for this model. The sharp decrease of the pressure near the surface emphasizes the interference of the direct and reflected shock waves, *Hood et al.* [2003] did not consider this reduction in their calculations. The shock demagnetization region, where the shock pressure is larger than 2 GPa, extends to a distance of about 80 km from the impact site. The entire 50 km thick surface layer is demagnetized within a radial distance of about 65 km (65% of the radius) from the impact site. Thermal demagnetization due to impact heating is not considered because the spatial extent of the thermal demagnetization is less than that of the shock demagnetization [*Mohit and Arkani-Hamed*, 2004].

[25] The effects of major parameters on the demagnetized region for an impact that creates a 200 km diameter crater are illustrated in Figure 9. The numbers 8, 10 and 12 on the curves denote the impact velocity. The single n value of 1.87 is used in these models. Within the impact velocity range considered, the demagnetized zone is less sensitive to the impact velocity. The model used for curve P = 3 GPa is identical to that used for curve 10, except for the demagnetizing pressure which is assumed to be 3 GPa. Likewise, the

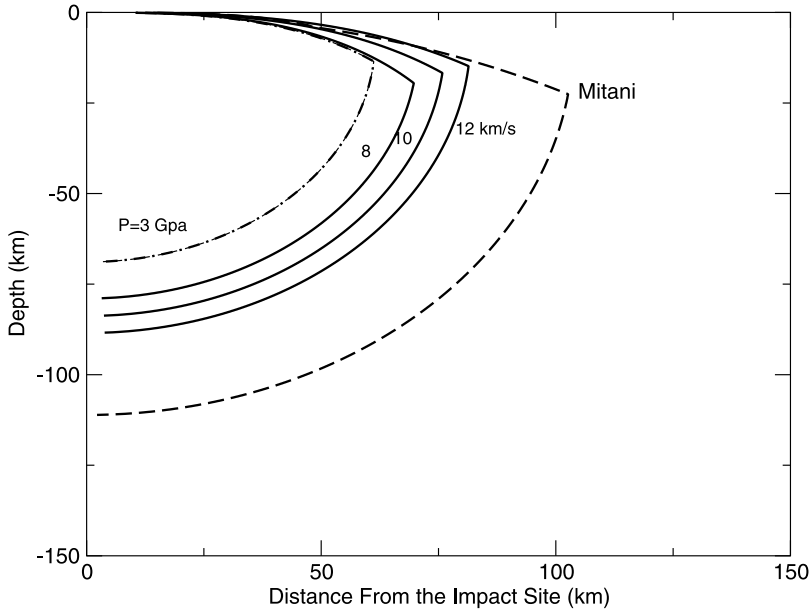

Figure 9. The demagnetized zones resulted from an impact that created a 200 km diameter crater. Inside of a given curve is the region where the shock pressure exceeds 2 GPa. The region is considered to be completely demagnetized by the shock wave. The numbers on the solid curves denote the impact velocity (km/s). The pressure in the region inside curve p = 3 GPa exceeds 3 GPa. The curve denoted by Mitani is calculated using *Mitani*'s [2003] exponent n values. The pressure in the region inside this curve exceeds 2 GPa.

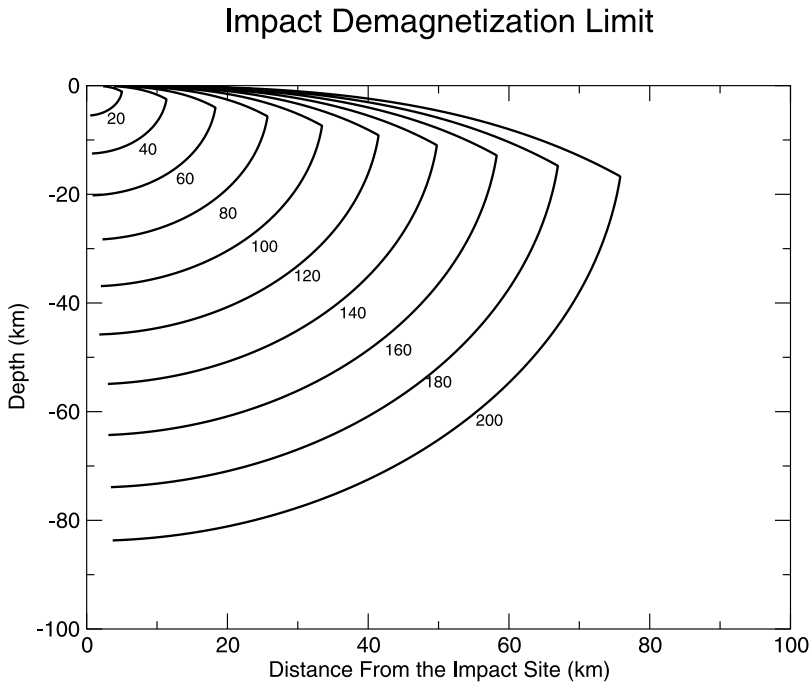

Figure 10. The demagnetized zones resulted from impact that created craters of 20–200 km diameter. The inside of a given curve denotes the region where the shock pressure exceeds 2 GPa. The numbers on the curves are the diameter of the resulting craters.

model used for curve Mitani is identical to that used for curve 10 but the variable n values of *Mitani* [2003] are adopted. The fully demagnetized region is more extensive for Mitani's model and least extensive for the demagnetizing critical pressure of 3 GPa than that of the demagnetizing critical pressure of 2 GPa.

[26] Figure 10 shows the demagnetized zones, where pressure exceeds 2 GPa, due to impacts that produce different size craters. The single n value of 1.87 and an impact velocity of 10 km/s are used in these models. The numbers on the curves denote the resulting crater diameters. Note that the curves are not concentric. The center of each curve is defined by the depth of penetration of the projectile from the surface, taken as the radius of the projectile [*Melosh*, 1989]. In reality the near surface region within the transition diameter is largely excavated and partly disturbed with random orientations, even though it is not subject to high shock pressures, as emphasized by *Melosh* [1989]. This region retains no coherent direction of its previous magnetization and thus has no appreciable contribution to the observed magnetic anomalies. We assume that this region is completely demagnetized. Equation (9) shows that the transition diameter is comparable to the resulting crater diameter for small craters, but it decreases rapidly as the crater diameter increases. Impacts larger than about 100 km are capable of demagnetizing a large portion of the crust within a fraction of radius from the center of the craters. The observation by *Frey et al.* [2002] indicates that the density distribution of buried craters is comparable to that of the visible, implying appreciable demagnetization by visible and buried impact craters. The figure suggests that aside from large impacts that have likely demagnetized the entire crust the uppermost 10–20 km of the crust has been almost completely demagnetized through gardening by impacts that have created visible and buried craters of diameters smaller than 100 km. Scaling ~25 km highly fractured mega regolith of the low gravity Moon [*Simmons et al.*, 1973; *Goins et al.*, 1981] to the higher gravity Mars suggests that the possible mega regolith of Mars can be around 10–15 km, which is comparable to the above mentioned 10–20 km.

[27] Many craters with diameters 250–500 km that are capable of demagnetizing the entire crust within 60–80% of the radius show almost no effects of demagnetization [*Mohit and Arkani-Hamed*, 2004]. It is quite possible that the craters are created over already demagnetized upper curst. But this does not avoid further demagnetization of the deeper regions by larger impacts. The resulting demagnetization depends on the coercivity of the major magnetic minerals. *Cisowski and Fuller* [1978] found that remanence with a coercivity of 70 mT was ~20% demagnetized after a shock of 1 GPa and 70% after a shock of 4 GPa. Single domain magnetite and multidomain hematite also have high coercivities [*Kletetschka et al.*, 2000]. Under a shock of 1 GPa, the remanence of the lamellar magnetism, single-domain magnetite, and multidomain hematite and magnetite are reduced by 20%, 68%, 70%, and 85% respectively [*Kletetschka and Wasilewski*, 2002]. Low-coercivity titanomagnetite can be mostly demagnetized by shocks as low as 0.25 GPa [*Pohl et al.*, 1975]. At room temperature, the coercivity of pyrrhotite samples analyzed by *Menyeh and O'Reilly* [1995] varied from 38 mT (for a grain size of 23–26 μm) to 63 mT (for a grain size of 2–5 μm), but dropped linearly to zero as temperature increased toward the Curie point. Shock experiments on high coercivity (300 mT) single domain pyrrhotite samples showed that a shock of

1 GPa removed 50% of the magnetization at room temperature, and they were completely demagnetized by shocks exceeding 2.75 GPa, undergoing a transition to a paramagnetic phase [*Rochette et al.*, 2003]. It is possible that the magnetic carriers of the Martian crust have high coercivity and do not get demagnetized at pressures of 1–3 GPa [*Kletetschka et al.*, 2004]. It is also possible that magnetic anomalies are younger than the craters. The cratering history of Mars is not well understood, whether cratering was a more or less continuous process until it sharply reduced at about 4 Gyr ago or there was catastrophic cratering in the vicinity of 4 Ga [e.g., *Hartmann and Neukum*, 2001]. If the core dynamo ceased much later than the final period of intensive cratering (which is an open question) it is possible for intrusive bodies that penetrated the impact-demagnetized zone after the intensive cratering but before the cessation of the core dynamo, to acquire primary magnetization.

[28] There are numerous visible and buried craters of diameters greater than 300 on Mars [*Frey*, 2003; *Frey et al.*, 2001, 2002, 2003]. They are, however, less frequent and far from each other. Although an individual impact may have demagnetized the crust, the demagnetized regions are localized. The correlation of the observed magnetic anomalies with these craters provides a means to assess the depth of the magnetic source bodies and in some cases the age of the anomalies relative to the craters [*Shahnas and Arkani-Hamed*, 2005].

4. Secondary Magnetization of the Lower Crust

[29] The thermal remanent magnetization (TRM) of the potentially magnetic layer of Mars is acquired mainly during the active period of core dynamo and partly after the dynamo ceased to exist. Thermal evolution models presented in the previous section show that the upper part of the crust in all of the models cooled below the Curie temperature of its magnetic minerals and acquired TRM in the presence of the core field, called hereafter the primary magnetization. The lower parts of the crust were either hot in the early history of Mars or became hot at later times, but then cooled below the Curie temperature of the magnetic minerals. It is possible that they acquired TRM in the presence of the magnetic field produced by the upper part of the crust, called hereafter as secondary magnetization. This possibility was examined by *Arkani-Hamed* [2003] using highly magnetic lower crust. He concluded that the secondary magnetization of the lower crust has minor contributions to the observed magnetic anomalies.

[30] The magnetization M acquired at a point in the crust in a weak magnetic field is linearly dependent on the field,

$$\mathbf{M} = \varepsilon \mathbf{B}, \tag{15}$$

where B is the ambient magnetic field and ε is the magnetization factor which is inversely proportional to saturation magnetization J [e.g., *Kletetschka et al.*, 2004] and reflects the magnetic properties of rocks. Lateral variations of magnetization, which give rise to the magnetic anomalies, may arise from lateral variations of B, or from lateral variations of ε, or both. *Arkani-Hamed* [2003] assumed that the upper crust was magnetized by a dipole core field, a very smooth and slowly varying field. The lateral variations of magnetization in the upper crust were due to the lateral variations of ε, i.e., the magnetic properties of the crustal rocks. On the other hand, he assumed a laterally uniform ε for the lower crust and allowed the lateral variations of the magnetic field of the upper crust to induce laterally varying magnetization in the lower crust, the stronger magnetic field induced stronger magnetization and vice versa. It is possible that certain regions of the lower crust are highly magnetic with large ε values and can acquire appreciable magnetization in a weak ambient field. For example, the magnetic source bodies in the upper crust may have roots in the lower crust. One scenario is that possibly large igneous plutons intruded the crust in the very early history of the planet and resulted in major mineralization. The upper parts of the plutons cooled below the Curie temperature during the active period of the core dynamo and acquired primary magnetization, while deeper parts cooled after the core dynamo ceased to exist. They acquired secondary magnetization in the presence of the magnetic field of the upper crust. Another scenario is that the lateral variations of magnetization in the crust, responsible for the observed magnetic anomalies, are due to juxtaposition of crustal blocks with different magnetic properties. The lower parts of a given block cooled below the Curie temperature after the core dynamo ceased to exist and acquired secondary magnetization. In both scenarios there seems to be a correlation between the locations of the source bodies in the upper crust and those in the lower crust. The correlation, however, is not straightforward, largely because the shape and magnetic properties of each pluton, or crustal block, are more likely depth dependent. Moreover, there is no reason to believe that mineralization in the lower crust was necessarily the same as the mineralization in the upper crust. For example, many deep seated plutons may not have even penetrated the upper crust. To take all these possibilities into account, it is sufficient to assume a layer in the lower crust with uniform but very high magnetization factor. Such a layer acquires a strong magnetization in the presence of a moderate magnetic field of the upper crust and resembles places with strong mineralization. *Arkani-Hamed* [2003] also examined this scenario, by considering a highly magnetic layer between 60 km and 75 km depth to represent the possible ilmenite-rich layer. It was assumed that the ilmenite-rich layer created highly magnetic ilmenite-hematite lamellae with a magnetization factor of 25 times that of the freshly produced oceanic basalt. He concluded that such a highly magnetic layer can have some contribution to the observed magnetic anomalies, but the contribution is still less than that of the primary magnetization of the upper crust.

[31] Another issue is the bulk primary magnetization of the upper crust that magnetized the lower crust. The relatively low crater density distribution inside the giant basins Hellas, Argyre and Isidis compared to that on the surrounding highlands suggests that intensive cratering predates the formation of the basins. The core dynamo also most likely ceased to exist before the formation of the basins [e.g., *Acuna et al.*, 1999; *Arkani-Hamed*, 2004]. Whether the dynamo ceased before or after the intensive cratering is not clear yet. It is, however, plausible to assume that the period between the cessation of the core field and

the intense cratering was likely short and that the lower crust did not cool appreciably during this short period. This suggests that the uppermost 10–20 km of the crust had likely been already demagnetized, through impact-induced shock waves discussed in the previous section, before the lower crust acquired its secondary magnetization.

[32] This paper extends *Arkani-Hamed*'s [2003] technique to include a demagnetized uppermost crust, as well as a highly magnetic layer directly beneath the upper crust. The highly magnetic layer introduced by Arkani-Hamed was located ~20 km below the upper crust and thus was relatively weakly magnetized by the magnetic field of the upper crust. Figure 7 shows that the upper ~80 of Mars was potentially magnetized by the core dynamo if magnetite is the major magnetic mineral. In the present study it is assumed that the upper 50 km acquired primary magnetization, but its uppermost region was later demagnetized by impacts. The thermal evolution models presented in the previous section show that the upper about 80 km of Mars was colder than the Curie temperature of magnetite during the active period of the core dynamo, capable of acquiring primary magnetization. But because of gradual accretion the crust may not have thickened as much [*Hauck and Phillips*, 2002], and this cold region may have included parts of the uppermost mantle. Whether the upper parts of the Martian mantle is magnetic and carries appreciable magnetization is not clear at present. The upper mantle of the Earth below continents is more likely nonmagnetic [e.g., *Wasilewski et al.*, 1979]. Moreover, the magnetization of the deeper parts of the crust that remained at temperatures close to the Curie temperature would decay through viscous demagnetization after the cessation of the core dynamo [*Shahnas and Arkani-Hamed*, 2005]. Taking for example 60 km, rather than 50 km, for the thickness of the upper crust that acquired primary magnetization has little effect on the bulk primary magnetization of the crust, and thus on the intensity of the secondary magnetization of the lower crust (see below). The lower crust cooled gradually below the magnetic blocking temperatures of its magnetic minerals. A given point in the lower crust was magnetized by the magnetic field of the remaining primarily magnetized upper crust plus the magnetic field arising from the secondary magnetization of the upper parts of the lower crust that had already cooled and acquired magnetization. The highly magnetic layer of the lower crust, directly beneath the upper crust, may represent a product of strong mineralization, as mentioned above. Because of its low Curie temperature, pyrrhotite cannot be a magnetic carrier of the highly magnetic layer of the uppermost lower crust. The TRM of coarse grain magnetite, >0.005 mm, is less than that of the coarse grain hematite, >0.1 mm [e.g., *Kletetschka et al.*, 2000]. Whether finer grain magnetite can be produced at high temperatures of the lower crust is not clear, but coarse grain hematite can be produced at such high temperatures. Let us consider coarse grain hematite for discussion purposes. A 0.1–1 mm grain size pure hematite acquires about 1000 A/m in 0.1 mT magnetic field [*Hartstra*, 1982; *Kletetschka et al.*, 2000], equivalent to ~350 A/m at the present geomagnetic equator of Earth. This is ~20 times greater than the average magnetization of the freshly produce oceanic basalt at the oceanic ridge axes in the equatorial region [e.g., *Bliel and Petersen*, 1983]. It is highly unlikely that the Martian core field was as strong as the Earth's, and even less likely that mineralization processes could result in pure hematite over tens to hundreds of thousands km^2 area, that is required to explain the magnetic anomalies associated with Cimmeria and Sirenum Terrae. The upper limit for possible hematite concentration is probably less than 50%. The magnetization factor of the highly magnetic layer must be much less than 20 times that of the freshly produced oceanic basalt.

Table 4. Parameters of the Secondary Magnetization Models[a]

Model	1	2	3	4	5
Nominal	10	40	0	0	4
2	10	40	0	0	40
3	10	40	1	5	80
4	20	30	0	0	4
5	20	30	0	0	40
6	20	30	1	5	80
7	0	50	0	0	4
8	0	50	0	0	40
9	0	50	1	5	80

[a]The columns are as follows: 1, the thickness of the near surface demagnetized zone (km); 2, the thickness of part of the upper crust with primary magnetization (km); 3, the index of magnetic properties of the lower crust (0, a magnetically uniform lower crust and 1, a heterogeneous lower crust with a highly magnetic layer); 4, the sublayer with enhanced magnetic properties (0, all sublayers are equally magnetic and 5, sublayer 5 is the highly magnetic sublayer); and 5, the magnetic properties of the lower crust (4, freshly produced oceanic basalt; 40, 10 times more magnetic than the basalt; and 80, sublayer 5 is 20 times more magnetic than the basalt, but the other sublayers are similar to the oceanic basalt).

[33] Several magnetization models (Table 4) are calculated to systematically investigate the contribution of the secondary magnetization of the lower crust to the observed magnetic anomalies of Mars. The thickness of the demagnetized near surface zone is set to 0, 10, or 20 km. The magnetization factor of the lower crust is taken to be 1 or 10 times that of the freshly produced oceanic basalt. The magnetization factor of the highly magnetic layer in the uppermost part of the lower crust is assumed to be 20 times greater than that of the oceanic basalt, equivalent to the magnetization factor of coarse grain pure hematite. These extreme values are examined in order to obtain an upper limit for the contribution of the lower crust to the observed magnetic anomalies. The primary magnetization of the upper crust is determined, through a generalized inversion method, such that the magnetization of the entire potentially magnetic layer gives rise to the observed magnetic anomalies of Mars (see *Arkani-Hamed* [2003] for detailed formulation). The depth to the bottom of the potentially magnetic layer at present is assumed to be at 100 km for all of the models, the upper 50 km carries primary magnetization except for the impact-demagnetized zone and the lower 50 km carries the secondary magnetization. If hematite is the major magnetic carrier, the potentially magnetic layer at present will be about 120 km. However, increasing the thickness of the potentially magnetic layer from 100 to 120 km, by adding 20 km to the bottom of the layer, has little effects on the contribution of the secondary magnetization of the lower crust to the observed magnetic anomalies (see below). The 100 km thick potentially magnetic layer adopted in this paper provides an upper limit for the contribution of the secondary magnetization of the lower crust to the observed magnetic anomalies

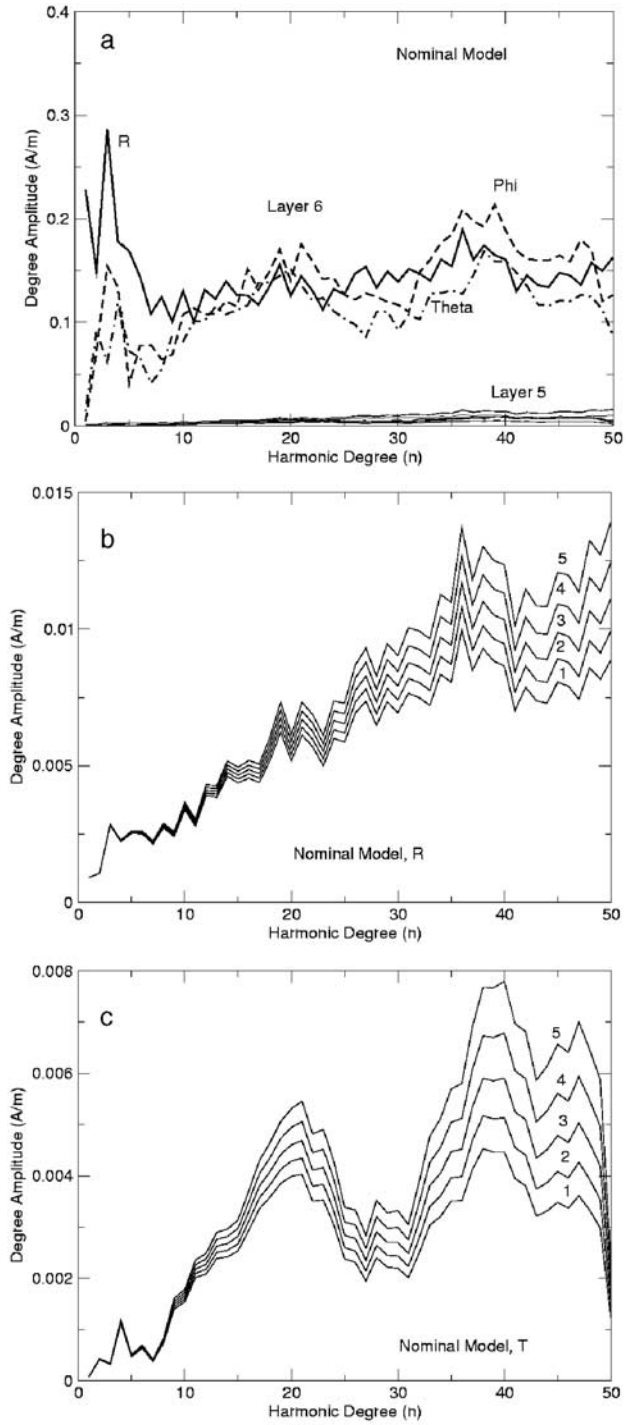

Figure 11. The amplitude spectra of the primary magnetization of the upper crust (Layer 6) and the secondary magnetization of sublayer 5 (Layer 5), located directly beneath the upper crust, of the nominal model. The entire lower crust has the same magnetic properties of the freshly produced oceanic basalt. (a) R, Theta, and Phi denote the radial, the north-south, and the east-west components of the magnetization, (b) the radial (R) component of the secondary magnetization, and (c) the north-south (T) component of the secondary magnetization. The numbers on the curves in Figures 11b and 11c are the sublayers in the lower crust that acquired secondary magnetization.

of Mars. For calculation purposes, the lower crust is divided into five equal sublayers of 10 km thickness, with equal magnetization factors for a given model. The sublayer 1 is the deepest sublayer and sublayer 5 is directly below 50 km depth. The latter represents the highly magnetic layer of the lower crust in those models with such a layer.

[34] Figure 11a shows the amplitude spectra of the vector components of the magnetization of the nominal model (see Table 4 for the new definition of the nominal model) in the upper crust, layer 6, which is magnetized by the core field, and in the sublayer 5 which carries secondary magnetization. The amplitude spectrum of a component of the magnetization vector, A_n, is determined by

$$A_n = \left[\Sigma_{m=0}^{n}\left(C_{nm}^2 + S_{nm}^2\right)\right]^{1/2}, \tag{16}$$

where C_{nm} and S_{nm} stand for the even and odd coefficients of the fully normalized spherical harmonic expansion of the vector component, respectively. The primary magnetization of the upper crust is dominant in this model. Figures 11b and 11c show the amplitude spectra of the magnetization of the sublayers, indicating that the lower sublayers are weakly magnetized compared to sublayer 5. Note that the lower crust of the model consists of highly magnetic materials similar to that of freshly produced oceanic basalt.

[35] Figures 12a and 12b show the amplitude spectra of the radial and north-south components of the primary magnetization of the upper crust for three different thicknesses of the impact-demagnetized near surface zone. The amplitude spectra of the east-west component (not shown here) are similar to those of the north-south component, though not identical. The demagnetized near-surface zone is 0 km thick for Model 5, 10 km thick for the nominal model, and 20 km thick for Model 6. The magnetizations of Model 5 and Model 6 are normalized such that their bulk magnetization (vertically integrated magnetization) is equal to that of the nominal model, for better comparison. The demagnetization of the near-surface zone has minor effects on the bulk magnetization of the upper crust, a thicker magnetic layer requires weaker magnetization and vice versa. The differences between the models at shorter wavelengths are quite small.

[36] Figure 13a shows the amplitude spectra of the magnetization vector components for the upper crust and sublayer 5, when the entire lower crust is 10 times more magnetic than freshly produced oceanic basalt (Model 2). The lower sublayers have weaker magnetization (not shown in the figure) compared to that of sublayer 5. The lower crust in this model is equivalent to a layer with 50% coarse grain hematite. Despite this highly magnetic lower crust, its secondary magnetization is less than the primary magnetization of the upper crust. Figure 13b is similar to Figure 13a but for Model 3, where all of the lower crust is similar to freshly produced oceanic basalt except for sublayer 5, which is 20 times more magnetic. This sublayer is equivalent to a layer of coarse grain pure hematite, a very highly mineralized layer. The long wavelength components of the primary magnetization of the upper crust are still stronger than those of the secondary magnetization of sublayer 5. At shorter wavelengths, however, the secondary magnetization of

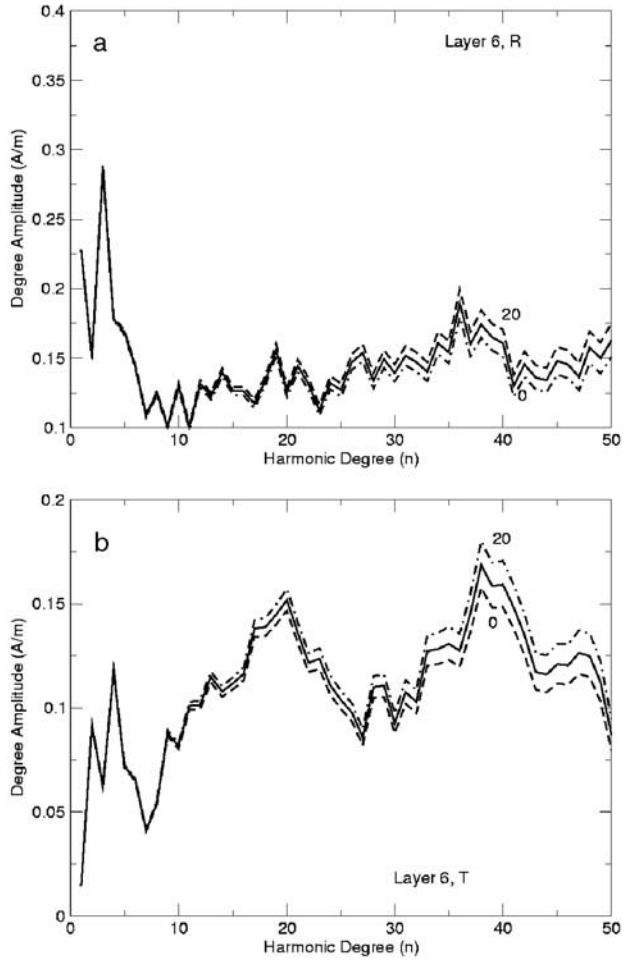

Figure 12. The amplitude spectra of the primary magnetization of the upper crust (Layer 6): (a) radial (R) component and (b) north-south (T) component. The numbers on the curves denote the thickness (km) of the impact-demagnetized uppermost crust. The solid curves are for the nominal model.

sublayer 5 is stronger than those of the primary magnetization of the upper crust. Nevertheless, the contribution of the sublayer 5 to the magnetic anomalies at 400 km altitude is still less than that of the upper crust over the entire wavelengths considered (see below).

[37] The lower crust has less contribution to the observed magnetic anomalies, not only because of its generally weaker magnetization but also because of its greater distance from the observation points. Figure 14 shows the contribution of sublayer 5 normalized to that of the upper crust (assuming both are equally magnetized) determined by

$$\lambda_n = \left[R_6^{n+2} - R_5^{n+2}\right] / \left[R_7^{n+2} - R_6^{n+2}\right], \qquad (17)$$

where R_5 and R_6 are the radii to the bottom and top of sublayer 5, and R_7 is the radius to the top of the primarily magnetized part of the upper crust. Numbers on the curves denote the thickness of the uppermost impact-induced demagnetized zone. Deeper sublayers have less contribution than sublayer 5. Note that because of severe attenuation of short wavelength components of the magnetic anomalies, the short wavelength components of the magnetization of sublayer 5 have much smaller contribution to the observed magnetic anomalies in all of the models. The primary magnetization of the upper crust is the main magnetic source of Mars, as was concluded by *Arkani-Hamed* [2003].

5. Discussion and Conclusions

[38] The locations of the magnetic source bodies that give rise to the strong magnetic anomalies over Cimmeria and Sirenum Terrae are mainly constrained by the thermal evolution of Mars and the impact demagnetization of the uppermost crust. The thermal evolution of Mars has constrained the depth to the bottom of the potentially magnetic layer. A total of 23 thermal evolution models of Mars are examined to determine the effects of eight major physical

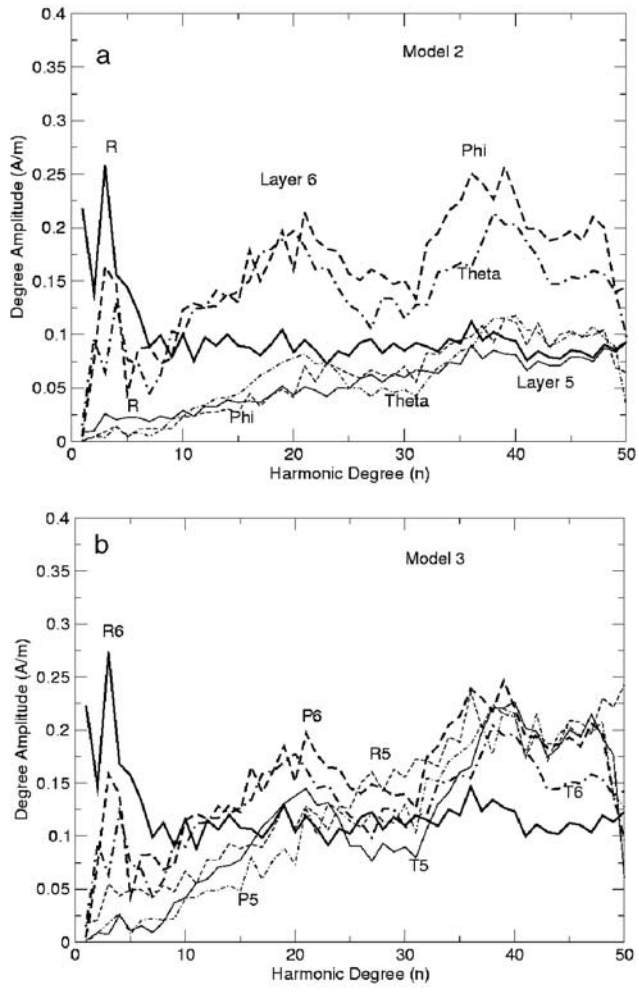

Figure 13. The amplitude spectra of the primary magnetization of the upper crust (Layer 6) and the secondary magnetization of the sublayer 5 (Layer 5), located directly beneath the upper crust, of the nominal model. (a) The entire lower crust is 10 times more magnetic than the freshly produced oceanic basalt. (b) The entire crust is as magnetic as the freshly produced oceanic basalt, except for sublayer 5, which is 20 times more magnetic. R (R), Theta (T), and Phi (P) denote the radial, the north-south, and the east-west components of the magnetization.

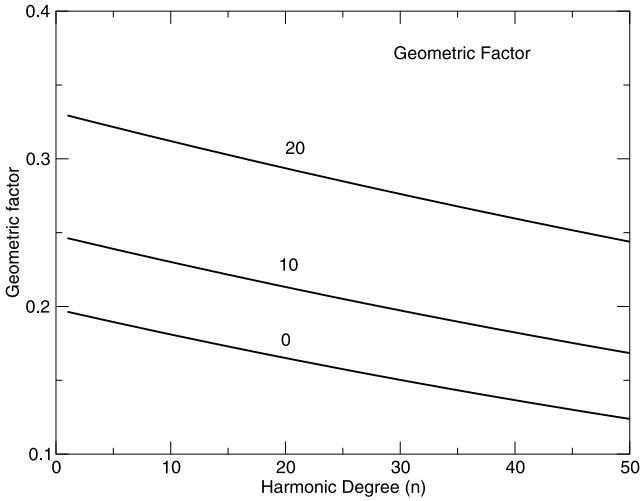

Figure 14. The contribution of sublayer 5, normalized to that of the upper crust, to the observed magnetic anomalies, assuming that both the upper crust and the sublayer are equally magnetized. The numbers on the curves denote the thickness of the impact-demagnetized zone (km). For example, the curve denoted by 20 has a 30 km thick upper crust (located between 20 and 50 km depths) which carries primary magnetization.

parameters on the thermal state of the Martian crust. The parameters include (1) the thickness of the initial crust created by chemical differentiation of a magma ocean; (2) the viscosity of the mantle; (3) the initial temperature in the upper mantle immediately after the creation of the initial crust; (4) the possible super heated core; (5) the total radioactive content at present and different Th/U and K/U ratios; (6) the total radioactive elements concentrated in the crust; (7) the total potassium concentrated in the core; and (8) the pressure dependence of the thermal expansion coefficient. The thermal evolution models are based on parameterized convection calculations with a growing stagnant lid on the convecting mantle. The lid initially consists of the crust and uppermost part of the mantle, but it thickens in time as the upper parts of the mantle cool. The potentially magnetic layer thins in the early stages of evolution in almost all models, because of higher content of the radioactive elements and, more importantly, hampering the heat loss from the interior by the stagnant lid. The magnetic source bodies that have been magnetized by the core field in the first about 500 Myr of the planet's history are located in the upper 100–90, 90–80, or 55–40 km of the crust if hematite, magnetite, or pyrrhotite is the major magnetic carrier.

[39] In the absence of any constraining data, thermal evolution models of Mars are highly model dependent, whether they are calculated by simple parameterized convection method as done in this paper and by many other investigators mentioned above, or by solving the actual mantle dynamic equations, where no rigorous constraints on the rheology and initial temperature of the mantle can be imposed because of our lack of pertinent information. The 23 models presented in this paper are surely not exhaustive. However, I examined a wide range of physical parameters in order to assess their effects on the potentially magnetic layer. The three important parameters, the initial temperature of mantle, the viscosity of the mantle and the total radioactive heat source content of Mars, span a wide range. The initial temperature in the upper mantle is within between the solidus and melting temperatures of peridotite [e.g., *Matsukage and Kubo*, 2003; *Lesher et al.*, 2003]. The radioactive content of the models spans a large range, from highly radioactive [*Lodders and Fegley*, 1997] to less radioactive [*Wänke and Dreibus*, 1994]. I also examined a terrestrial like radioactive content. For an upper mantle temperature of 1700 K two viscosity values 2×10^{19} and 10^{20} Pa s are examined. The main conclusion is that all models, except Model 5 and Model 14, result in a comparable depth to the bottom, about 80 km ± 10 km, of the potentially magnetic layer if magnetite is the magnetic carrier. This is thicker than the 50 km suggested by *Arkani-Hamed* [2003] on the basis of earlier parameterized convection models, where the base of the stagnant lid was set to a fixed elastic-to-ductile transition temperature of 1073 K, as was also adopted by many authors [e.g., *Stevenson et al.*, 1983; *Schubert and Spohn*, 1990]. This is much lower than the temperature, around 1500 K, calculated in the present paper using equation (7).

[40] The upper boundary of the potentially magnetic layer is constrained by the impact demagnetization effect. A total of 14 models are investigated to estimate the impact-induced shock pressure distribution in the lithosphere and the extent of shock demagnetization. It is shown that the impacts creating craters of diameter ~50 km are capable of demagnetizing the upper about 10–20 km of the crust. The ancient surface of Cimmeria and Sirenum Terrae has been heavily bombarded by such impact, implying that the magnetic source bodies in these regions are located deeper than 10–20 km. I also investigated the possibility that the lower parts of the crust acquired secondary thermal remanent magnetization as they cooled below the Curie temperature of their magnetic minerals in the absence of the core field but in the presence of the magnetic field generated by the upper parts of the crust. A total of 9 models are examined for the magnetic properties of the lower crust, which range from the magnetic properties of freshly produced oceanic basalt type material up to that of coarse grain pure hematite. Despite these extraordinary magnetic materials, it is demonstrated that the secondary magnetization of the lower crust has minor effects on the observed magnetic anomalies of Mars.

[41] The thickness of the potentially magnetic layer is identified in this study by the depth to the Curie temperature of magnetic carriers. This tends to overestimates the layer thickness, which is in accordance with the main goal of the paper that is to estimate the upper limit for the magnetic layer of Mars. Rocks usually acquire magnetization not exactly at the Curie temperature, but gradually within a range of magnetic blocking temperatures. The magnetic blocking temperatures of magnetite, hematite and pyrrhotite continuously vary from their Curie temperatures down to ~100 degrees lower than their Curie temperatures [*Dunlop and Özdemir*, 1997]. The temperature profiles in the stagnant lid during the first 500 Myr (Figure 4) shows that the entire range of the magnetic blocking temperatures occurs within ~20 km above the base of the magnetic layer. The effective thickness of the magnetic layer is less than the one

suggested from the depth to Curie temperature. But the difference is probably less than 20 km, because large portions of magnetization are acquired at blocking temperatures closer to the Curie temperature [*Dunlop and Özdemir*, 1997].

[42] There are distinct differences in the magnetic properties of the Earth and Mars. The magnetic anomalies of Earth's continents largely arise from the induced magnetization (IM) acquired in the presence of the core field. The intermediate and long wavelength magnetic anomalies of continents detected by magnetometers on POGO, Magsat, Oersted, and Champ satellites arise largely from the induced magnetization of the lower crust [e.g., *Schnetzler and Allenby*, 1983; *Mayhew*, 1985]. The upper about 15–20 km of the crust is dominated by low magnetic sedimentary structures, whereas the lower crust is largely gabbroic with appreciable magnetic susceptibility almost everywhere, and it is magnetically enhanced, partly because of the increase in magnetic susceptibility at higher temperatures close to the Curie temperature of magnetic minerals. The magnetic anomalies over the continents are mainly produced by lateral heterogeneities introduced in the lower crust [e.g., *Frey*, 1982; *Arkani-Hamed and Strangway*, 1985]. The juxtaposition of tectonic provinces with different magnetic properties, such as the highly magnetic Archaean cratons and the surrounding low magnetic mobile belts, produce appreciable magnetic anomalies. For example, the Central Africa and Liberia cratons in Africa and Anabar and Olomon cratons in Asia have large magnetic anomalies (see *Arkani-Hamed and Strangway* [1985] for the locations of the places mentioned here). Such is also the case for some large basins with Archaean cratonic floors such as Tarim, Szechwan and Shansi basins in Asia. The continent-continent collision zones whether old or young (for example, the Thelon front and Grenville Front in North America, the Alps in Europe, the Himalayas in Asia, and the Zagross mountains in Iran) are low magnetic zones, possibly because the underlying high-magnetic lower crust has been suppressed into high temperature mantle through the collision processes and has been thermally demagnetized. Several young rifts, for example, the Amazon elacogen and Takutu rift in South America and Afar uplift in Africa, have low magnetization, likely because of the partial demagnetization of the lower crust due to the high temperature of newly intruded hot material. The Kursk iron formation in Ukraine is very extensive and has created a very large magnetic anomaly. It is not, however, clear to what extent the remanent magnetization has contributed to its anomaly. Although remanent magnetization could be dominant at some local regions [e.g., *Kletetschka and Stout*, 1998] there is no evidence that it dominates over larger areas and thus is responsible for the magnetic anomalies detected at satellite altitudes of about 400 km.

[43] The magnetic anomalies of Mars are produced by lateral variations in the remanent magnetization of the crust. The upper 10–20 km of the crust is severely demagnetized by impact-induced shock waves. The magnetic source bodies are located within 10–60 km depths in the crust. However, it does not seem that this part of the crust is more or less globally magnetic similar to the lower crust of the Earth. It is worth mentioning that the potentially magnetic crust of Mars does not necessarily indicate that the entire crust is magnetic and has acquired magnetization as it cooled in the presence of the core field. Rather the low temperatures in the crust provide a suitable place for intrusive bodies, which formed much later than the crust, to cool below the Curie temperature of their magnetic minerals and acquire magnetization. The lack of appreciable magnetic anomalies over about 1/3 of the southern highlands as well as over the highlands surrounding the northern lowlands in the northern hemisphere implies very low magnetic crust in those regions. It is not possible to determine whether the strong magnetic anomalies of the southern hemisphere are due to juxtaposition of crustal blocks with strongly different magnetization, or they are related to extensive mineralization by large plutons. One of the major difficulties with detailed geological interpretation of the Martian magnetic anomalies is their low resolution. Geological features with wavelengths shorter than 400 km cannot be well resolved by the existing magnetic data of Mars [*Purucker and Arkani-Hamed*, 2004]. This severely limits the geological interpretation of the anomalies, as demonstrated for the aeromagnetic anomalies of eastern Canada acquired at about 300 m altitude [*Zheng and Arkani-Hamed*, 1998]. There are numerous small and irregular magnetic anomalies on the 300m-altitude magnetic map. Upward continuing the anomalies to 100 km altitude severely decreases their amplitudes while the anomalies combine to produce extended but smooth anomalies. The anomalies almost totally disappear at higher altitudes. Even larger anomalies are diminished at higher altitudes. For example, the well-defined Grenville front, created through the continent-continent collision process at about 900 Myr ago, is well delineated on the aeromagnetic map as a low magnetic zone running from east Canada down to southern USA almost parallel to the ocean-continent boundary. The feature is still visible when the map is upward continued to 100 km altitude, but looses its integrity at 200 km altitude and more so at 400 km altitude. This emphasizes the fact that it is impossible with the available magnetic data to decide whether the strong anomalies over Cimmeria and Sirenum Terrae are manifestations of similar tectonic features, or they are due to large plutons.

[44] **Acknowledgments.** This research was supported by the Natural Sciences and Engineering Research Council (NSERC) of Canada. I would like to thank Gunther Kletetschka and an anonymous reviewer for their useful comments.

References

Acuna, M. H., et al. (1999), Global distribution of crustal magnetization discovered by the Mars Global Surveyor MAG/ER experiment, *Science*, *284*, 790–793.

Arkani-Hamed, J. (2000), Strength of Marian lithosphere beneath large volcanoes, *J. Geophys. Res.*, *105*, 26,713–26,732.

Arkani-Hamed, J. (2001), Paleomagnetic pole positions and pole reversals of Mars, *Geophys. Res. Lett.*, *28*, 3409–3412.

Arkani-Hamed, J. (2002), Magnetization of the Martian crust, *J. Geophys. Res.*, *107*(E5), 5032, doi:10.1029/2001JE001496.

Arkani-Hamed, J. (2003), Thermoremanent magnetization of the Martian lithosphere, *J. Geophys. Res.*, *108*(E10), 5114, doi:10.1029/2003JE002049.

Arkani-Hamed, J. (2004), Timing of the Martian core dynamo, *J. Geophys. Res.*, *109*, E03006, doi:10.1029/2003JE002195.

Arkani-Hamed, J., and D. W. Strangway (1985), Intermediate-scale magnetic anomalies of the Earth, *Geophysics*, *50*, 2817–2830.

Blichert-Toft, J., J. D. Gleason, P. Télouk, and F. Albarède (1999), The Lu-Hf isotope geochemistry of shergottites and the evolution of the Martian crust-mantle system, *Earth Planet. Sci. Lett.*, *173*, 25–39.

Bliel, U., and N. Petersen (1983), Variations in magnetization intensity and low-temperature titanomagnetite oxidation of ocean floor basalts, *Nature*, *301*, 384–388.

Borg, L. E., L. E. Nyquist, L. A. Taylor, H. Wiesmann, and C.-Y. Shih (1997), Constraints on Martian differentiation processes from Rb-Sr and Sm-Nd isotopic analyses of the basaltic shergottite QUE 94201, *Geochim. Cosmochim. Acta*, *61*, 4915–4931.

Breuer, D., and T. Spohn (2003), Early plate tectonics versus single-plate tectonics on Mars: Evidence from magnetic field history and crust evolution, *J. Geophys. Res.*, *108*(E7), 5072, doi:10.1029/2002JE001999.

Cisowski, S. M., and M. Fuller (1978), The effect of shock on the magnetism of terrestrial rocks, *J. Geophys. Res.*, *83*, 3441–3458.

Connerney, J. E. P., et al. (1999), Magnetic lineations in the ancient crust of Mars, *Science*, *284*, 749–798.

Connerney, J. E. P., M. H. Acuna, P. J. Wasilewski, G. Kletetschka, N. F. Ness, H. Remes, R. P. Lin, and D. L. Mitchell (2001), The global magnetic field of Mars and implications for crustal evolution, *Geophys. Res. Lett.*, *28*, 4015–4018.

Dunlop, D. J., and J. Arkani-Hamed (2005), Magnetic minerals in the Martian crust, *J. Geophys. Res.*, doi:10.1029/2005JE002404, in press.

Dunlop, D. J., and G. Kletetschka (2001), Multidomain hematite: A source of planetary magnetic anomalies?, *Geophys. Res. Lett.*, *28*, 3345–3348.

Dunlop, D. J., and Ö. Özdemir (1997), *Rock Magnetism: Fundamentals and Frontiers*, 573 pp., Cambridge Univ. Press, New York.

Frey, H. V. (1982), Magsat scalar anomaly distribution: The global perspective, *Geophys. Res. Lett.*, *9*, 277–280.

Frey, H. V. (2003), Large-diameter visible and buried impact basins on Mars: Implications for age of the highlands and buried lowlands and turn-off of the global magnetic field, *Proc. Lunar Planet. Sci. Conf. 34th*, abstract 1838.

Frey, H., K. M. Shockey, E. L. Frey, J. H. Roark, and S. E. H. Sakimoto (2001), A very large population of likely buried impact basins in the northern lowlands of Mars revealed by MOLA data, *Proc. Lunar Planet. Sci. Conf. 32nd*, abstract 1680.

Frey, H. V., J. H. Roark, K. M. Shockey, E. L. Frey, and S. E. H. Sakimoto (2002), Ancient lowlands on Mars, *Geophys. Res. Lett.*, *29*(10), 1384, doi:10.1029/2001GL013832.

Frey, H. V., E. L. Frey, W. K. Hartmann, and K. L. T. Tanaka (2003), Evidence for buried ''Pre-Noachian'' crust pre-dating the oldest observed surface units on Mars, *Proc. Lunar Planet. Sci. Conf. 34th*, abstract 1848.

Goins, N. R., A. M. Daintly, and M. N. Toksoz (1981), Lunar seismology: The internal structure of the Moon, *J. Geophys. Res.*, *86*, 5061–6074.

Grasset, O., and E. M. Parmentier (1998), Thermal convection in a volumetrically heated, infinite Prandtl number fluid with strongly temperature-dependent viscosity: Implications for planetary thermal evolution, *J. Geophys. Res.*, *103*, 18,171–18,181.

Halliday, A. N., H. Wanke, J.-L. Birk, and R. N. Clayton (2001), The accretion, composition and early differentiation of Mars, *Space Sci. Rev.*, *96*, 197–230.

Hargraves, R. B., J. M. Knudson, M. B. Madsen, and P. Bertelsen (2001), Finding the right rocks on Mars, *Eos Trans. AGU*, *82*, 292–293.

Harper, C. L., Jr., L. E. Nyquist, B. Bansal, H. Wiesmann, and C.-Y. Shih (1995), Rapid accretion and early differentiation of Mars indicated by $^{142}Nd/^{144}Nd$ in SNC meteorites, *Science*, *267*, 213–217.

Harrison, C. G. A. (2000), Questions about magnetic lineations in the ancient crust of Mars, *Science*, *287*, 547a.

Hartmann, W., and G. Neukum (2001), Cratering chronology and the evolution of Mars, *Space Sci. Rev.*, *96*, 165–194.

Hartstra, R. L. (1982), Grain-size dependence of initial susceptibility and saturation magnetization-related parameters of four natural magnetites in the PSD-MD range, *Geophys. J. R. Astron. Soc.*, *71*, 477–495.

Hauck, S. A., II, and R. J. Phillips (2002), Thermal and crustal evolution of Mars, *J. Geophys. Res.*, *107*(E7), 5052, doi:10.1029/2001JE001801.

Holsapple, K. A. (1993), The scaling of impact processes in planetary sciences, *Annu. Rev. Earth Planet. Sci.*, *21*, 333–373.

Hood, L. L., and N. Richmond (2002), Mapping and modeling of major magnetic anomalies, *Proc. Lunar Planet. Sci. Conf. 33rd*, Abstract 1128.

Hood, L. L., N. C. Richmond, E. Pierazzo, and P. Rochette (2003), Distribution of crustal magnetic fields on Mars: Shock effects of basin-forming impacts, *Geophys. Res. Lett.*, *30*(6), 1281, doi:10.1029/2002GL016657.

Jagoutz, E. (1991), Chronology of SNC meteorites, *Space Sci. Rev.*, *56*, 13–22.

Kletetschka, G., and J. H. Stout (1998), The origin of magnetic anomalies in lower crustal rocks, Labrador, *Geophys. Res. Lett.*, *25*(2), 199–202.

Kletetschka, G., and P. J. Wasilewski (2002), Low-level shock in magnetite, titanohematite and hematite, *Eos Trans. AGU*, *83*(19), Spring Meet. Suppl., Abstract P41A-08.

Kletetschka, G., P. J. Wasilewski, and P. T. Taylor (2000), Mineralogy of the sources for magnetic anomalies on Mars, *Meteorit. Planet. Sci.*, *35*, 895–899.

Kletetschka, G., P. J. Wasilewski, and P. T. Taylor (2002), The role of hematite-ilmenite solid solution in the production of magnetic anomalies in ground and satellite based data, *Tectonophysics*, *347*, 166–177.

Kletetschka, G., J. E. P. Connerney, N. F. Ness, and M. H. Acuna (2004), Pressure effects on Martian crustal magnetization near large impact basins, *Meteorit. Planet. Sci.*, *39*, 1839–1848.

Kletetschka, G., N. F. Ness, J. E. P. Connerney, M. H. Acuna, and P. J. Wasilewski (2005), Grain size dependent potential for self generation of magnetic anomalies, *Phys. Earth Planet. Inter.*, *148*, 149–156.

Langlais, B., M. E. Purucker, and M. Mandea (2004), Crustal magnetic field of Mars, *J. Geophys. Res.*, *109*, E02008, doi:10.1029/2003JE002048.

Lesher, C. E., J. Pickering-Witter, G. Baxter, and M. Walter (2003), Melting of garnet peridotite: Effects of capsules and thermocouples, and implications for the high-pressure mantle solidus, *Am. Miner.*, *88*, 1181–1189.

Lodders, K., and B. Fegley (1997), An oxygen isotope model for the composition of Mars, *Icarus*, *126*, 373–394.

Matsukage, K. N., and K. Kubo (2003), Chromian spinel during melting experiments of dry peridotite (KLB-1) at 1.0–2.5 GPa, *Am. Miner.*, *88*, 1271–1278.

Mayhew, M. A. (1985), Curie isotherm surfaces inferred from high altitude magnetic anomaly data, *J. Geophys. Res.*, *90*, 2647–2654.

McDonough, W. F., and S.-S. Sun (1995), The composition of the Earth, *Chem. Geol.*, *120*, 223–253.

McGovern, P. J., S. C. Solomon, D. E. Smith, M. T. Zuber, M. Simons, M. A. Wieczorek, R. J. Phillips, G. A. Neumann, O. Aharonson, and J. W. Head (2002), Localized gravity/topography admittance and correlation spectra on Mars: Implications for regional and global evolution, *J. Geophys. Res.*, *107*(E12), 5136, doi:10.1029/2002JE001854.

McLennan, S. C. (2001), Crustal heat production and the thermal evolution of Mars, *Geophys. Res. Lett.*, *28*, 4019–4022.

Melosh, H. J. (1989), *Impact Cratering: A Geologic Process*, Oxford Univ. Press, New York.

Menyeh, A., and W. O'Reilly (1995), The coercive force of fine particles of monoclinic pyrrhotite (Fe_7S_8) studied at elevated temperature, *Phys. Earth Planet. Inter.*, *89*, 51–62.

Mitani, N. K. (2003), Numerical simulations of shock attenuation in solids and reevaluation of scaling law, *J. Geophys. Res.*, *108*(E1), 5003, doi:10.1029/2000JE001472.

Mohit, P. S., and J. Arkani-Hamed (2004), Impact demagnetization of the Martian crust, *Icarus*, *168*, 305–317.

Moresi, L. N., and V. S. Solomatov (1995), Numerical investigation of 2D convection with extremely large viscosity variations, *Phys. Fluids*, *7*, 2154–2162.

Neukum, G., and D. V. Wise (1976), Mars: A standard crater curve and possible new time scale, *Science*, *194*, 1381–1387.

Nimmo, F., and M. S. Gilmore (2001), Constraints on the depth of magnetized crust on Mars from impact craters, *J. Geophys. Res.*, *106*, 12,315–12,323.

Nimmo, F., and D. J. Stevenson (2000), Influence of early plate tectonics on the thermal evolution and magnetic field of Mars, *J. Geophys. Res.*, *105*, 11,969–11,979.

Norman, M. D. (1999), The composition and thickness of the crust of Mars estimated from rare earth elements and neodymium-isotopic compositions of Martian meteorites, *Meteorit. Planet. Sci.*, *34*, 439–449.

Norman, M. D. (2002), Thickness and composition of the Martian crust revisited: Implications of an ultradepleted mantle with a Nd isotope composition like that of QUE94201, *Proc. Lunar Planet. Sci. Conf. 33rd*, Abstract 1175.

Pohl, J., U. Bliel, and U. Hornemann (1975), Shock magnetization and demagnetization of basalt by transient stress up to 10 kbar, *J. Geophys. Res.*, *41*, 23–41.

Purucker, M., and J. Arkani-Hamed (2004), Resolving power of satellite magnetic data for lithospheric field characterization, *Eos Trans. AGU*, *85*(47), Fall Meet. Suppl., Abstract GP31A-0824.

Robinson, P., R. J. Harrison, S. A. McEnroe, and R. Hargrave (2002), Lamellar magnetism in the hematite-ilmenite series as an explanation for strong remanent magnetization, *Nature*, *418*, 517–520.

Rochette, P., G. Fillion, R. Ballou, F. Brunet, B. Ouladdiaf, and L. Hood (2003), High pressure magnetic transition in pyrrhotite and impact demagnetization on Mars, *Geophys. Res. Lett.*, *30*(13), 1683, doi:10.1029/2003GL017359.

Schatz, J. F., and G. Simmons (1972), Thermal conductivity of earth materials at high temperatures, *J. Geophys. Res.*, *77*, 6966–6983.

Schmidt, R. M., and K. R. Housen (1987), Some recent advances in the scaling of impact an explosion cratering, *Int. J. Impact Eng.*, *5*, 543–560.

Schnetzler, C. C., and R. J. Allenby (1983), Estimation of lower crustal magnetization from satellite derived anomaly field, *Tectonophysics*, *93*, 33–45.

Schubert, G., and T. Spohn (1990), Thermal history of Mars and the sulfur content of its core, *J. Geophys. Res.*, *95*, 14,095–14,101.
Shahnas, H., and J. Arkani-Hamed (2005), Demagnetization of Martian crust, paper presented at Canadian Geophysical Union Meeting, Banff, Canada.
Simmons, G., T. Todd, and H. Wang (1973), The 25-km discontinuity: Implications for lunar history, *Science*, *182*, 158–161.
Sleep, N. H. (1994), Martian plate tectonics, *J. Geophys. Res.*, *99*, 5639–5665.
Sohl, F., and T. Spohn (1997), The interior structure of Mars: Implications form SNC meteorites, *J. Geophys. Res.*, *102*, 1613–1635.
Solomatov, V. S. (1995), Scaling of temperature- and stress-dependent viscosity convection, *Phys. Fluids*, *7*, 166–274.
Solomon, S. C., and J. W. Head (1990), Heterogeneities in the thickness of the elastic lithosphere of Mars: Constraints on heat flow and internal dynamics, *J. Geophys. Res.*, *95*, 11,073–11,083.
Spohn, T., M. H. Acuna, D. Breuer, M. Golombek, R. Greeley, A. Halliday, E. Hauber, R. Jaumann, and F. Sohl (2001), Geophysical constraints on the evolution of Mars, *Space Sci. Rev.*, *96*, 231–262.
Stengel, K. C., D. S. Oliver, and J. R. Booker (1982), Onset of convection in a variable-viscosity fluid, *J. Fluid Mech.*, *120*, 411–431.
Stevenson, D. J., T. Spohn, and G. Schubert (1983), Magnetism and thermal evolution of the terrestrial planets, *Icarus*, *54*, 466–489.
Turcotte, D. L., and G. Schubert (1982), *Geodynamics*, 450 pp., John Wiley, Hoboken, N. J.
Turcotte, D. L., R. Shcherbakov, B. D. Malamud, and A. B. Kucinskas (2002), Is the Martian crust also the Martian elastic lithosphere?, *J. Geophys. Res.*, *107*(E11), 5091, doi:10.1029/2001JE001594.
Van Hoolst, T., V. Dehant, and P. Defraigne (2000), Sensitivity of the free core nutation and the Chandler wobble to changes in the interior structure of Mars, *Phys. Earth Planet. Inter.*, *117*, 397–405.
Voorhies, C. V., T. J. Sabaka, and M. Purucker (2002), On magnetic spectra of Earth and Mars, *J. Geophys. Res.*, *107*(E6), 5034, doi:10.1029/2001JE001534.
Wänke, H., and G. Dreibus (1994), Chemistry and accretion of Mars, *Philos. Trans. R. Soc. London, Ser. A*, *349*, 2134–2137.
Wasilewski, P. J., H. H. Thomas, and M. A. Mayhew (1979), The Moho as a magnetic boundary, *Geophys. Res. Lett.*, *6*, 541–544.
Zheng, Y., and J. Arkani-Hamed (1998), Joint inversion of gravity and magnetic anomalies of eastern Canada, *Can. J. Earth Sci.*, *35*, 832–853.
Zuber, M. T., et al. (2000), Internal structure and early thermal evolution of Mars from Mars Global Surveyor topography and gravity, *Science*, *287*, 1788–1793.

J. Arkani-Hamed, Earth and Planetary Sciences, McGill University, 3450 University Street, Montreal, Quebec, Canada H3A 2A7. (jafar@eps.mcgill.ca)